OPEN ACCESS

UNIVERSITY OF BRISTOL

Peer reviewed version

License (if available):
Other

Link to published version (if available):
10.1142/S0218127419300155

Link to publication record in Explore Bristol Research
PDF-document

University of Bristol - Explore Bristol Research
General rights

Micro-slip as a loss of determinacy
in dry friction oscillators

Mike R. Jeffrey, Simon Webber

University of Bristol

November 15, 2018

Abstract

Dry-friction contacts in mechanical oscillators can be modelled using nonsmooth differential equations, and recent advances in dynamical theory are providing new insights into the stability and uniqueness of such oscillators. A classic model is that of spring-coupled masses undergoing stick-slip motion on a rough surface. Here we present a phenomenon in which multiple masses transition from stick to slip almost simultaneously, but suffer a brief loss of determinacy in the process. The system evolution becomes many-valued, but quickly collapses back down to an infinitesimal set of outcomes, a sort of 'micro-indeterminacy'. Though fleeting, the loss of determinacy means masses may each undergo different microscopic sequences of slipping events, before all masses ultimately slip. The microscopic loss of determinacy is visible in local changes in friction forces, and in creating a bistability of global stick-slip oscillations. If friction forces are coupled between the oscillators then the effect is more severe, as solutions are compressed instead onto two (or more) macroscopically different outcomes.

1   Introduction

In nonsmooth dynamics, differential equations are permitted to suffer discontinuities due to, for example, physical parameters that change between different media, forces that switch abruptly, perhaps due to changes in rigid body contacts, opening of valves, changes in environment, and so on. Dry friction oscillator models, in particular, are used to gain insight into brake wear and automotive stability [9, 54, 13], oil drill stick-slip [38, 34], and geological motion in behind earthquakes [12, 8, 40, 10, 24] or glacial

slippage [46]. Although a simple low dimensional model of a dry friction oscillator —
essentially a block slipping and sticking on some moving surface — is not intended
to capture all of the complexity of an automobile or a tectonic plate, such models
do reveal discontinuity-induced phenomena with significant consequences for stability
and determinacy in such applications, particularly wor systems with several parts or
multiple contacts.

The general behaviour of such systems is the subject of *piecewise-smooth dynamical
systems* theory. Much traditional work focussed on discovering conditions for the exis-
tence and uniqueness of solutions of piecewise-smooth equations. The requirement of
uniqueness is somewhat difficult to ensure in the presence of discontinuities, and there
exist many situations where it does not hold. Here we describe a novel phenomenon
whereby solutions become non-unique, and though this occurs for a vanishingly small
interval of time, the effects can be seen in broken determinacy on a global scale. We
present the phenomenon in the context of a pair of coupled oscillators experiencing
static friction on a moving surface, suffering a momentarity break in determinism at
the instant when either block is able to slip. After local geometric analysis we simulate
the system by smoothing out the discontinuity and adding noise-like perturbations, to
illustrate the phenomenon's effect in a less ideal model with compliance and noise.

Solutions in nonsmooth systems can find themselves evolving along thresholds of dis-
continuity — a behaviour called 'sliding' which represents, for example, frictional stick-
ing in mechanics. As solutions enter into sliding they collapse onto a lower dimensional
space of motion, making them irreversible. Solutions can also escape from sliding
into higher dimensions, and in doing so become non-unique in forward time, breaking
determinacy. Solutions of a dynamic problem can be found as follows.

If the rate of change of some variable y suffers a discontinuity, say $\dot{y} = a(y) +
b(y)\operatorname{sign}(y)$, then we study the dynamics at the discontinuity surface $y = 0$ by 'blowing
it up' into a *switching layer* $y \in [-\varepsilon, +\varepsilon] \to 0$ for $\varepsilon \to 0+$. Inside the layer we find
fast dynamics effecting the fast jump across the discontinuity, but this can also be
interrupted by invariant manifolds, places where $\dot{y} = 0$ inside $y \in [-\varepsilon, +\varepsilon]$, which trap
the dynamics inside the layer, hence inside the discontinuity surface, and so produce
'sliding' or sticking motion along the discontinuity.

Our main interest here is on the forms that these *sliding manifolds* can take, and the
implications of manifolds losing stability, which happens when they fold with respect
to the fast switching flow, fig. 1. At such a fold, sliding solutions can escape from the
attracting branch of the invariant manifold, in to the fast flow, and thence exit the
switching layer to begin regular slipping motion outside the discontinuity surface. The
typical local picture is shown in fig. 1, and will be derived in section 3.

Taking a system of two oscillators gives a vector field containing two discontinuity
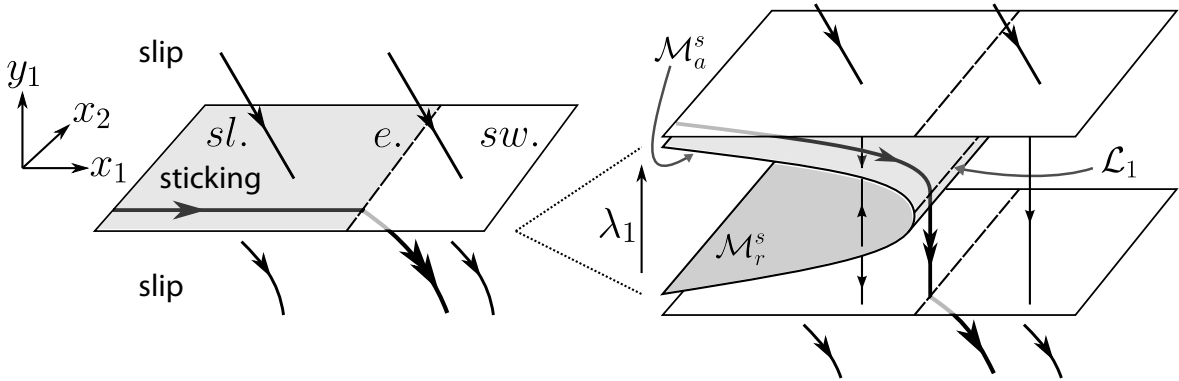
2

Figure 1: A sketch demonstrating a fold of a sliding manifold in $\mathbb{R}^3$. In the left figure *sl.* labels a stable sliding region, *sw.* labels a region where solutions switch from the upper to lower vector field, and between them is a line *e.* where solutions exit from sliding into the lower vector field. The right figure shows the blow-up of the discontinuity surface into a switching layer $y_1 \in [-\varepsilon, +\varepsilon]$, by letting $y_1 = \varepsilon\lambda_1$ for some small ε. In the layer the sliding region reveals two branches of a sliding manifold, one attracting $\mathcal{M}_a^s$ and one repelling $\mathcal{M}_r^s$. These make up the sliding manifold $\mathcal{M} = \mathcal{M}_a^s \cup \mathcal{M}_r^s$, and they join along a line $\mathcal{L}_1$ from which solutions are able to escape from sliding on $\mathcal{M}_a^s$, exit the layer and begin slipping. A single trajectory demonstrating this behaviour is shown in bold. Throughout the paper, double headed arrows are used to indicate a trajectory exiting the sliding manifold.

surfaces, due to friction terms proportional to $\text{sign}(y_1)$ and $\text{sign}(y_2)$ where y_1 and y_2 are the oscillator velocities. These will typically intersect at $y_1 = y_2 = 0$, illustrated in fig. 2 (the figure is essentially a generalization of fig. 1 but only a partial representation of a four-dimensional phase space can be shown — its features wiill be explained throughout the course of this paper). When we blow up the discontinuity surfaces the switching layer around this intersection is then two-dimensional, $(y_1, y_2) \in [-\varepsilon, +\varepsilon]^2$ for some small ε. This contains fast dynamics, and typically contains a sliding manifold when $\dot{y}_1 = \dot{y}_2 = 0$, which corresponds to both oscillators undergoing sticking at $y_1 = y_2 = 0$. The manifold can now fold over with respect to either or both directions in the layer, and exit from sliding can occur along the individual folds (labelled $\mathcal{L}_1$ and $\mathcal{L}_2$ in fig. 2). The exit is similar to fig. 1, but solutions must pass through the neighbouring single switching layers before ultimately exiting the discontinuity surfaces altogether (shown by light grey trajectories in fig. 2).

More unusual behaviour occurs as a result of the manifold turning over with respect to both directions simultanously, at the corner $\mathcal{L}_1 \cap \mathcal{L}_2$ in fig. 2. The exit is then set-valued, and fig. 2 illustrates the different possibilities schematically (to be derived in detail in section 4). The loss of determinacy means the sequence by which the two blocks exit from stick to slip, and their phase space trajectories afterwards, are multi-valued. This determinacy breaking is illustrated in fig. 2 by the bold trajectory on $\mathcal{M}_a^{ss}$ exploding into the entire shaded set as it passes through the singularity $\mathcal{L}_1 \cap \mathcal{L}_2$. However, as

the solution set evolves into the neighbouring layer systems (corresponding to one or other block sticking only), the system re-stabilizes by collapsing these many solution into a vanishingly (as $\varepsilon \to 0$) small region, confining the breakdown of determinism to the $\mathcal{O}(\varepsilon)$ scale. All trajectories thus reach the same slipping trajectory, albeit by microscopically (i.e. $\mathcal{O}(\varepsilon)$) different routes.
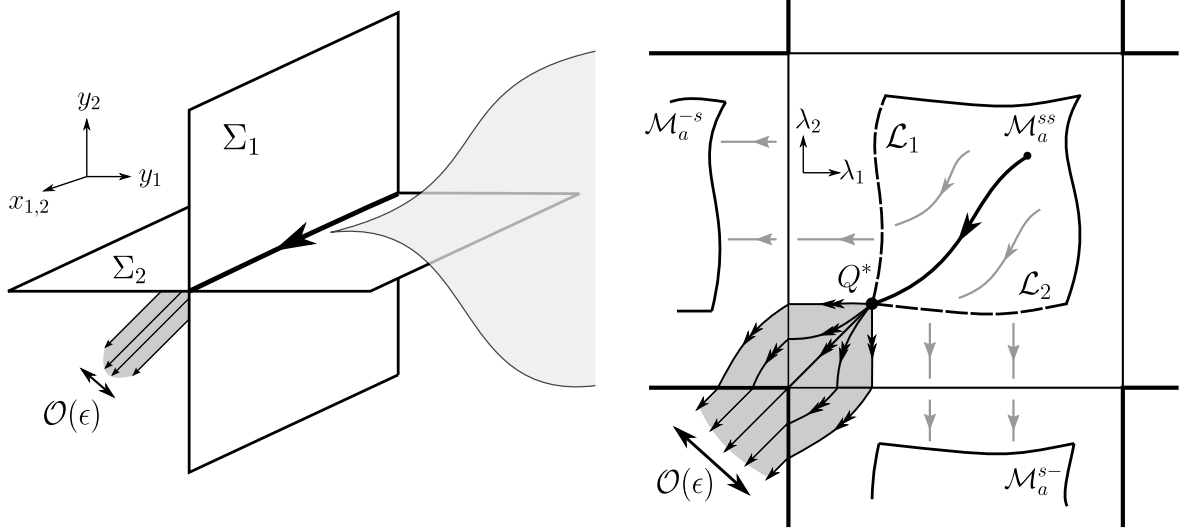

Figure 2: A sketch demonstrating schematically how the breakdown of determinism occurs at the kind of singularity we study here. The right hand sketch is of the layer systems present local to the intersection of two discontinuities, $\Sigma_1 \cap \Sigma_2$, shown on the left. Grey trajectories leave $\mathcal{M}_a^{ss}$ along either of the folds $\mathcal{L}_1$ or $\mathcal{L}_2$ and are attracted to $\mathcal{M}_a^{s-}$ or $\mathcal{M}_a^{-s}$ respectively via the fast flows. On both sketches, the single trajectory that crosses the intersection of the folds is shown in black; after passing through $\mathcal{L} \cap \mathcal{L}_2$ it becomes set-valued as it loses determinism.

The microscopic confinement of the loss of determinacy is a result of the decoupled friction forces of the mechanical oscillators. We will show that the indeterminacy becomes macroscopically observable in the presence of coupling. We will also prove that the phenomenon persists if the discontinuity is smoothed out, and hence is not an artefact of a nonsmooth friction model.

In principle the loss of determinacy could lead to one or other block sticking for a sustained interval of time, while the other slips, in an unpredictable manner (finding a new sliding manifold, e.g. $\mathcal{M}_a^{s-}$ or $\mathcal{M}_a^{-s}$ in fig. 2, in the layers around either $y_1 = 0$ or $y_2 = 0$).

Steps towards a classification of the generic scenarios of such exit from slipping were made in [28], showing that solutions exit from sliding deterministically if they encounter no change in attractivity of a sliding manifold, and showing some simple scenarios whereby changes in attractivity led to non-deterministic exit. This classification

included the case of the simple fold in fig. 1, for example, but did not conceive of the kind of microscopic burst of indeterminacy found here.

The paper is set out as follows. We recount the basic techniques for studying dynamics across the discontinuity in section 2, and for demonstration we apply it to a single oscillator in section 3. We then study the phenomenon of micro-indeterminacy in the context of two oscillators in section 4. Simulations of global dynamics induced by the interminacy are given in section 5, and we make some final remarks on the generalization of the effect in section 7.

2 Resolving dynamics in a switching layer

Consider a system of variables $\boldsymbol{x} = (x_1, x_2, ...)$ and $\boldsymbol{y} = (y_1, y_2, ...)$, with a set of quantities $\boldsymbol{\lambda} = (\lambda_1, \lambda_2, ...)$, on $\boldsymbol{x} \in \mathbb{R}^n$, $\boldsymbol{y} \in \mathbb{R}^m$, $\boldsymbol{\lambda} \in [-1, +1]^m$. Let the dynamics on $\boldsymbol{x}$ and $\boldsymbol{y}$ be described by

$$\begin{cases} \dot{\boldsymbol{x}} &= \boldsymbol{f}(\boldsymbol{x}, \boldsymbol{y}; \boldsymbol{\lambda}) \,, \\ \dot{\boldsymbol{y}} &= \boldsymbol{g}(\boldsymbol{x}, \boldsymbol{y}; \boldsymbol{\lambda}) \,, \end{cases} \tag{1}$$

where

$$\lambda_i = \text{sign}(y_i) \,, \qquad i = 1, ..., m \,. \tag{2}$$

We let $\text{sign}\, 0 \in \mathbb{L}$ where, throughout this paper, $\mathbb{L}$ denotes the real interval $(-1, +1)$ and $\bar{\mathbb{L}}$ denotes its closure,

$$\mathbb{L} = (-1, +1) \,, \qquad \bar{\mathbb{L}} = [-1, +1] \,. \tag{3}$$

Let us briefly set out the methods used to analyze such a system from [26, 27, 30], which develop on methods in [19, 52].

On each $y_j = 0$, to describe how each λ_j evolves across the interval $\text{sign}(0) \in \bar{\mathbb{L}}$, we can let $y_j = \varepsilon_j \lambda$ for some non-negative ε_j; this method follows [26, 30]. As we let $\varepsilon_j \to 0$, the variation inside the interval $\lambda_j \in \bar{\mathbb{L}}$ is squashed onto the discontinuity surface $y_j = 0$, which effects the switch between $\lambda_j = -1$ for $y_j < 0$ and $\lambda_j = +1$ for $y_j > 0$. This is known as *blowing up* the discontinuity surface

$$\Sigma = \{(\boldsymbol{x}, \boldsymbol{y}) \in \mathbb{R}^{n+m} \ : \ y_1 = ... = y_m = 0\}$$

into a switching layer

$$\hat{\Sigma} = \{(\boldsymbol{x}, \boldsymbol{\lambda}) \in \mathbb{R}^n \times \mathbb{L}^m\} \quad \text{on } y_1 = ... = y_m = 0 \,. \tag{4}$$

Substituting $y_j = \varepsilon_j \lambda$ into (1) gives the *layer system*

$$\begin{cases} \dot{\boldsymbol{x}} & = \boldsymbol{f}(\boldsymbol{x}, \boldsymbol{E}.\boldsymbol{\lambda}; \boldsymbol{\lambda}) = \boldsymbol{f}(\boldsymbol{x}, 0; \boldsymbol{\lambda}) + \mathcal{O}(|\boldsymbol{E}|) \,, \\ \boldsymbol{E}.\dot{\boldsymbol{\lambda}} & = \boldsymbol{g}(\boldsymbol{x}, \boldsymbol{E}.\boldsymbol{\lambda}; \boldsymbol{\lambda}) = \boldsymbol{g}(\boldsymbol{x}, 0; \boldsymbol{\lambda}) + \mathcal{O}(|\boldsymbol{E}|) \,, \end{cases} \tag{5}$$

on $(\boldsymbol{x}, \boldsymbol{\lambda}) \times \mathbb{R}^n \times \mathbb{L}^m$, where $\boldsymbol{E} = diag(\varepsilon_1, ..., \varepsilon_m)$. For this paper it is enough to assume $\varepsilon_1 = ... = \varepsilon_m$ and relabel these simply $\varepsilon = \varepsilon_j$, then

$$\begin{cases} \dot{\boldsymbol{x}} & = \boldsymbol{f}(\boldsymbol{x}, \varepsilon\boldsymbol{\lambda}; \boldsymbol{\lambda}) = \boldsymbol{f}(\boldsymbol{x}, 0; \boldsymbol{\lambda}) + \mathcal{O}(\varepsilon) \,, \\ \varepsilon\dot{\boldsymbol{\lambda}} & = \boldsymbol{g}(\boldsymbol{x}, \varepsilon\boldsymbol{\lambda}; \boldsymbol{\lambda}) = \boldsymbol{g}(\boldsymbol{x}, 0; \boldsymbol{\lambda}) + \mathcal{O}(\varepsilon) \,, \end{cases} \tag{6}$$

Re-scaling to a new time $\tau = t/\varepsilon$ and denoting the derivative with respect to τ by a prime, we have the *fast system*

$$\begin{cases} \boldsymbol{x}' & = \varepsilon\boldsymbol{f}(\boldsymbol{x}, \varepsilon\boldsymbol{\lambda}; \boldsymbol{\lambda}) = \mathcal{O}(\varepsilon) \,, \\ \boldsymbol{\lambda}' & = \boldsymbol{g}(\boldsymbol{x}, \varepsilon\boldsymbol{\lambda}; \boldsymbol{\lambda}) = \boldsymbol{g}(\boldsymbol{x}, 0; \boldsymbol{\lambda}) + \mathcal{O}(\varepsilon) \,, \end{cases} \tag{7}$$

These three elements form the basis of our piecewise-smooth analysis: the external vector fields given by (1) on $(\boldsymbol{x}, \boldsymbol{y}) \in \mathbb{R}^{n+m}$ with each $\lambda_j = \pm 1$, the layer system (6) on $(\boldsymbol{x}, \boldsymbol{\lambda}) \times \mathbb{R}^n \times \mathbb{L}^m$, and the fast system (7) similarly on $(\boldsymbol{x}, \boldsymbol{\lambda}) \times \mathbb{R}^n \times \mathbb{L}^m$. In terms of the mechanics, the equations (1) describe dynamics while the blocks are slipping with speeds $y_j \neq 0$. When the slipping speeds y_j for each block vanish, either the blocks stick to the surface and follow the equations (6), or they quickly reverse slipping direction according to the fast equations (7).

In each of these regimes the equations can be solved using standard methods of dynamical systems theory. The methods are reminiscent of standard methods in singular perturbation theory for multiple timescale systems (e.g. [18, 33, 36]), but it must be remembered here that we are interested solely in the limit $\varepsilon \to 0$, and in the connection between different regions of dynamics internal or external to different switching layers, not in the singular perturbation to $\varepsilon > 0$. (We will, however, show in section 5 that our main results in this paper persist for $\varepsilon > 0$).

What happens is, in essence, that solutions evolve through the external fields (1) until they reach the discontinuity surface, when one or more of the variables y_j vanish. Let us take first the case where all $y_j = 0$. There we form a switching layer, by blowing up the discontinuity surface by means of a transformation $y_j = \varepsilon\lambda_j$, for each y_j that vanishes. Within the layer system, solutions first evolve on the fast timescale of (7). They either pass through the layer and hence cross through the discontinuity, or they encounter a fixed point of the fast subsystem where $\boldsymbol{g} = 0$. Those fixed points form an $\boldsymbol{x}$-parameterized set called the sliding manifold, identical to the set of points to which system (6) is constrained when we let $\varepsilon \to 0$. Hence dynamics evolves on the

6

t timescale, sliding along the manifold according to (6) with $\boldsymbol{g} = 0$, while the sliding manifold remains invariant.

The sliding manifold $\mathcal{M} = \{(\boldsymbol{x}, \boldsymbol{\lambda}) \times \mathbb{R}^n \times \mathbb{L}^m \; : \; \boldsymbol{g}(\boldsymbol{x}, 0; \boldsymbol{\lambda}) = 0\}$ is invariant so long as it remains normally hyperbolic (where the eigenvalues of the Jacobian matrix $\partial \boldsymbol{g}/\partial \boldsymbol{\lambda}$ have non-zero real part) and remains inside the layer (4). When either of these fail, solutions can exit from sliding, back into the fast flow of (7), there to be conveyed back into external dynamics describes by (1).

This description assumes all $y_j = 0$. If only one or more y_js vanish then we blow up only those surfaces $y_j = 0$ via $y_j = \varepsilon_j \lambda_j$, with all other y_i for $i \neq j$ being treated like the x_is in (6), and taking fixed values $\lambda_i = \text{sign}(y_i)$.

In terms of the mechanics, the equations (1) describe dynamics while the blocks are slipping with speeds $y_j \neq 0$. When the slipping speeds y_j for each block vanish, either the blocks stick to the surface and follow the equations (6), or they quickly reverse according to the fast equations (7).

These are essentially the methods we shall apply to one oscillator in section 3 and to two oscillators in section 4.

3   One Oscillator

Our main interest in this paper is a singularity that arises in a model of dry friction oscillators. Dry-friction has been a key motivating application in the study of dynamical systems with discontinuities since the early work of [1, 19], and remain a source of novel insights into nonsmooth phenomena, see e.g. [6, 4, 16, 35]. Dry friction oscillators have been particularly prominent, including single oscillators [17, 47, 14, 44, 41, 22, 23], and more recently coupled oscillators [20, 7, 2, 3]. There are a vast range of approaches to modeling the novel aspects of friction beyond the Coulomb model, such as friction memory and stiction, captured by nonlinear terms of one kind or another, see e.g. [15, 42, 21, 55, 56, 45]. The possibility of including static friction or *stiction* as nonlinear (or 'hidden') terms of a piecewise-smooth model was introduced in [31, 27].

The singularity we will be studying is a direct extension of a singularity that occurs for a single oscillator so, in preparation, let us begin there.

Consider a block, attached to a fixed wall by a spring of constant k and extension x, and a damper of coefficient ρ. The block sits on a rough surface that is moving at a constant speed v, experiencing a friction force F. The mass of the block can be scaled

out (included in the other constants), giving a system

$$\begin{cases} \dot{x} = f(x, y; \lambda) & = y + v \\ \dot{y} = g(x, y; \lambda) & = -kx - \rho(y + v) - F \end{cases}$$ (8)

A friction model $F = \mu \, \text{sign}(y)$ would represent Coulomb friction. Instead we take a model

$$F = F(\lambda) = \lambda\mu - \lambda\beta(\lambda^2 - 1) \,,$$ (9)

in terms of a discontinuous quantity $\lambda = \text{sign}(y)$, with $\beta > \mu/2$. This coincides with the Coulomb model for nonzero speeds $y \neq 0$. During sticking the friction force can vary over $F \in [-\frac{2(\beta+\mu)^{3/2}}{3\sqrt{3\beta}}, +\frac{2(\beta+\mu)^{3/2}}{3\sqrt{3\beta}}]$ at $y = 0$ for $\beta > \mu/2$, as we vary λ over $\lambda = \text{sign}(0) \in \bar{\mathbb{L}}$. By doing so (9) exhibits idealized static friction by overshooting the kinetic coefficient of friction μ when $y = 0$.

To analyse the dynamics at the discontinuity surface, $y = 0$, we use the methods from section 2. We identify λ as a blow up coordinate at $y = 0$ by making the mapping $y = \varepsilon\lambda$ for non-negative ε. We study the dynamics on $\lambda \in \bar{\mathbb{L}}$, which then corresponds to $y \in [-\varepsilon, +\varepsilon] \to 0$ as $\varepsilon \to 0$. Simply substituting $y = \varepsilon\lambda$ into (15) and omitting terms of order ε on the righthand side, we obtain

$$\begin{cases} \dot{x} = f(x, 0; \lambda) & = v \,, \\ \varepsilon\dot{\lambda} = g(x, 0; \lambda) & = -kx - \rho v - \lambda\mu + \lambda\beta(\lambda^2 - 1) \end{cases}$$ (10)

Taking the limit $\varepsilon \to 0$ this becomes a differential-algebraic system

$$\begin{cases} \dot{x} = f(x, 0; \lambda) & = v \,, \\ 0 = g(x, 0; \lambda) & = -kx - \rho v - \lambda\mu + \lambda\beta(\lambda^2 - 1) \,, \end{cases}$$ (11)

prescribing dynamics inside the layer constrained to the sliding manifold

$$\mathcal{M} = \left\{ x \in \mathbb{R}, \lambda \in \bar{\mathbb{L}} \; : \; \lambda = \lambda_0, \; g(x, 0; \lambda_0) = 0 \right\} \,,$$ (12)

shown in fig. 3. The curve defined by $\mathcal{M}$ is best visualised as lying in (x, λ) space on the cubic graph

$$x = X(\lambda_0) := \left(-\rho v - \lambda\mu + \lambda\beta(\lambda^2 - 1) \right)/k \,.$$

This exists for $X^- \leq x \leq X^+$, where $X^{\pm} = \left(-\rho v \pm \frac{2(\beta+\mu)^{3/2}}{3\sqrt{3\mu}} \right)/k$.

The dynamics outside $\mathcal{M}$ is found by re-scaling to the fast timescale $\tau = t/\varepsilon$, giving

$$\begin{cases} x' = 0 \,, \\ \lambda' = g(x, 0; \lambda) & = -kx - \rho v - \lambda\mu + \lambda\beta(\lambda^2 - 1) \,, \end{cases}$$ (13)

8

a family of scalar fast subsystems on λ, shown by the vertical flow in fig. 3, now parameterized by x as well as the constants k, ρ, μ, β. This fast system has steady states at values $\lambda = \lambda_0$, defined as the cubic roots of $g(x, 0; \lambda_0) = 0$, the set of which form precisely the sliding manifold $\mathcal{M}$. Then $\mathcal{M}$ consists of three branches of equilibria of the fast subsystem: attracting branches in $\frac{\mu/\beta+1}{3} < \lambda_0^2 < 1$, and a repelling branch in $\lambda_0^2 < \frac{\mu/\beta+1}{3}$, connected points at $\lambda_0^2 = \frac{\mu/\beta+1}{3}$ where the equilibria are neither hyperbolically attracting nor repelling. These stability properties follow from the eigenvalue of the fixed points,

$$\left. \frac{\partial g(x, 0; \lambda)}{\partial \lambda} \right|_{\lambda=\lambda_0(x)} = -\mu + \beta(3\lambda_0^2(x) - 1) , \tag{14}$$

which vanishes at $\lambda^\pm = \pm\sqrt{\frac{\mu/\beta+1}{3}}$, where the attracting and repelling equilibria on $\mathcal{M}$ come together in folds.

These different elements are illustrated in fig. 3.

Solutions may evolve through three different modes: slipping, fast switching, and sliding. The first describes slipping of the block on the surface when $y \neq 0$, leftwards if $\lambda = -1$ and rightwards if $\lambda = +1$, prescribed by (15). If a slipping solution reaches $y = 0$, the block is stationary with respect to the surface, and the friction force F begins rapidly changing as λ evolves according to (13). Either the system transitions directly between left/right slip via this fast switching, or, if $-\mu - \rho v < kx < +\mu - \rho v$, it encounters the manifold $\mathcal{M}$. Sliding then ensues according to (11).

We then come to the main point of interest in this paper (once we extend it to two oscillators). Assuming $v > 0$, a sliding solution will evolve until it reaches the point where normal hyperbolicity of the sliding manifold vanishes, at the fold (X^-, λ^-). The only forward continuation of the trajectory is then to re-enter the fast system (13), and evolve toward $\lambda = -1$, and thence into leftward slip, $y < 0$.

For a single oscillator the resulting dynamics, obtained by concatenating solutions of the systems (15) to (13), is therefore rather simple, and moreover is unique in forward time, i.e. it is deterministic (though it is not unique in backward time due to the way many solutions converge in finite time onto $\mathcal{M}^s$). This forward time determinacy breaks down when we look at two coupled oscillators.

4   Two Oscillators

We now reach our main subject of interest, and begin by extending the analysis above to two blocks, labelled $i = 1, 2$. Let each block be connected to a fixed wall by springs with constants k_1 and k_2, with $\boldsymbol{x} = (x_1, x_2)$ denoting their extensions, and by dampers
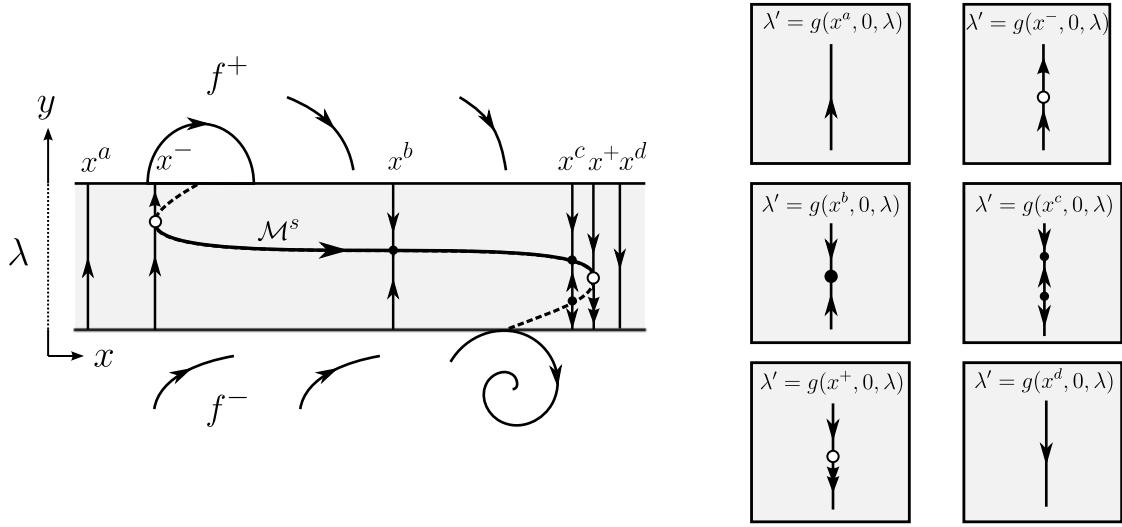
9

Figure 3: The phase portrait for the one oscillator system (15) featuring the layer system on $y = 0$. The corresponding fast subsystem inside the layer is shown at 6 different values of x, demonstrating different typical behaviours: at $x = x_a$ and $x = x_d$ there are no fixed points in the fast flow so trajectories switch quickly from left to right slip or *vice versa*; at $x = x_b$ there exists a single stable fixed point; at $x = x_c$ there exists one stable and unstable fixed point; and at $x = x^\pm$ these coaselesce in a fold bifurcation. Together these fixed points form $\mathcal{M}^s$, and the non-hyperbolic points are its folds.

both with coefficient ρ. Then $\boldsymbol{y} = (y_1, y_2) = (\dot{x}_1 - v, \dot{x}_2 - v)$ denotes the block velocities relative to some surface moving at speed v, on which they experience a friction force F, and we use the same friction model as in section 3. Let the two blocks also be coupled by a third spring with constant k_{12}. Then

$$\begin{cases} \dot{x}_i = f_i(\boldsymbol{x}, \boldsymbol{y}; \boldsymbol{\lambda}) & = y_i + v \ , \\ \dot{y}_i = g_i(\boldsymbol{x}, \boldsymbol{y}; \boldsymbol{\lambda}) & = -k_i x_i - k_{12}(x_i - x_j) - \rho(y_i + v) - F(\lambda_i) \ , \end{cases} \tag{15}$$

for $i = 1, 2$, $j = 2, 1$, with $\boldsymbol{\lambda} = (\lambda_1, \lambda_2)$ and $\lambda_i = \text{sign}(y_i)$, where F is defined as in (9).

Denote the two discontinuity surfaces in the system as

$$\Sigma_i = \{(\boldsymbol{x}, \boldsymbol{y}) \in \mathbb{R}^4 \ : \ y_i = 0\} \ , \qquad i = 1, 2, \tag{16}$$

and denote their intersection as

$$\Sigma_{12} = \Sigma_1 \cap \Sigma_2 = \{(\boldsymbol{x}, \boldsymbol{y}) \in \mathbb{R}^4 \ : \ y_1 = y_2 = 0\} \ . \tag{17}$$

This leaves us with five separate regions of the discontinuity surface on which we need to resolve the dynamics using the methods of section 2: the three-dimensional surface Σ_1 in $y_2 > 0$ and $y_2 < 0$, the three-dimensional surface Σ_2 in $y_1 > 0$ and $y_1 < 0$, and

10

the two-dimensional surface Σ_{12} connecting them. These correspond to the surfaces where block 1 is sticking while block 2 is slipping right or left, block 2 is sticking while block 1 is slipping right or left, and both blocks are sticking, respectively. Our main interest will be the latter.

We begin the analysis of the oscillator by separating out several subsystems on different timescales or different subspaces of the overall phase space. These different ingredients are then brought together in section 4.C to form a full picture of the resulting dynamics.

4.A   The layer system on Σ_{12} (both blocks sticking)

On the surface Σ_{12} where both blocks are sticking, following section 2 we blow the surface up into a layer

$$\hat{\Sigma}_{12} = \left\{ (\boldsymbol{x}, \boldsymbol{\lambda}) \in \mathbb{R}^2 \times \mathbb{L}^2 \right\} \quad \text{on } \boldsymbol{y} = \boldsymbol{0} \,. \tag{18}$$

The dynamics inside the layer is obtained by letting $y_i = \varepsilon \lambda_i$ for $\varepsilon \to 0$. Neglecting terms of order ε on the righthand side, this gives

$$\begin{cases} \dot{x}_i = f_i(\boldsymbol{x}, \boldsymbol{0}; \boldsymbol{\lambda}) & = v \,, \\ \varepsilon \dot{\lambda}_i = g_i(\boldsymbol{x}, \boldsymbol{0}; \boldsymbol{\lambda}) & = -k_i x_i - k_{12}(x_i - x_j) - \rho v - \lambda_i \mu + \lambda_i \beta(\lambda_i^2 - 1) \,, \end{cases} \tag{19}$$

for $i = 1, 2$, $j = 2, 1$, on the switching layer $(\boldsymbol{x}, \boldsymbol{\lambda}) \in \mathbb{R}^2 \times \mathbb{L}^2$. This is a four-dimensional two-timescale system consisting of slow variables (x_1, x_2) and fast variables (λ_1, λ_2). (More generally we could let $y_i = \varepsilon_i \lambda_i$ for $\varepsilon_1 \neq \varepsilon_2$ with $\varepsilon_i \to 0$, without altering the local dynamics of interest here provided ε_1 and ε_2 are of similar order, i.e. $\varepsilon_1/\varepsilon_2$ is finite at $\varepsilon_i \to 0$.)

We will show the following.

Proposition 1. *Micro-indeterminacy occurs in the system* (15) *if there exists a point*

$$Q_* = \left\{ (x_1, x_2, \lambda_1, \lambda_2) \in \mathbb{R}^2 \times \mathbb{L}^2 \; : \; x_i = X_i^-, \; \lambda_i = \lambda^-) \right\} \,, \tag{20}$$

on $y_1 = y_2 = 0$, *in terms of quantities* X_1^-, X_2^-, λ^-, *to be defined, such that:*

1. *there exists a one dimensional family of orbits of* (15) *that evolve into* Q_* *in finite time;*

2. *trajectories of* (15) *exit from* Q_* *in finite time such that they leave the switching layer on* $y_1 = y_2 = 0$ *via a set of points where* $(\lambda_1, \lambda_2) \in [-1, \lambda^-]^2$;

3. *those trajectories then evolve into either of the switching layers on* $y_i = 0 > y_j$ *where* $i \neq j$, *and evolve to* $\lambda_j = -1$, *with their speed* y_j *collapsing onto* $y_j = \mathcal{O}(\varepsilon)$ *as they do so.*

11

Thus trajectories exist that pass through the point Q_* in the sticking state on $y_1 = y_2 = 0$, and these explode into infinitely many possible trajectories as one of the y_js becomes nonzero (start slipping), but immediately these collapse down to an $\mathcal{O}(\varepsilon)$ set of values. The proposition will be formalized more completely in lemma 3, lemma 4, lemma 6 below.

I   The fast subsystem

Re-scaling to the fast timescale $\tau = t/\varepsilon$ in (19) and letting $\varepsilon \to 0$, yields

$$\begin{cases} x_i' = 0 \,, \\ \lambda_i' = g_i(\boldsymbol{x}, \boldsymbol{0}; \boldsymbol{\lambda}) \quad = -k_i x_i - k_{12}(x_i - x_j) - \rho v - \lambda_i \mu + \lambda_i \beta(\lambda_i^2 - 1) \,, \end{cases} \tag{21}$$

for $i = 1, 2$, $j = 2, 1$. This is a family of two-dimensional fast subsystems inside the switching layer, parametrised by the quasi-static quantities $\boldsymbol{x} = (x_1, x_2)$.

The fast subsystem (λ_1, λ_2) possesses an $\boldsymbol{x}$-parameterized family of equilibria, the set of which comprises the sliding manifold

$$\mathcal{M}^{ss} = \left\{ (\boldsymbol{x}, \boldsymbol{\lambda}) \in \mathbb{R}^2 \times \mathbb{L}^2 \; : \; \boldsymbol{g}(\boldsymbol{x}, \boldsymbol{0}; \boldsymbol{\lambda}) = 0 \right\} . \tag{22}$$

This surface represents states in which both blocks are sticking to the surface, since $g_i = 0 \Rightarrow \dot{\lambda}_i = 0 \Leftrightarrow \dot{y}_i = 0$, hence the double 's' superscript; later we will find corresponding surfaces $\mathcal{M}^{s\pm}$ and $\mathcal{M}^{\pm s}$ where only one block is sticking, indicated by 's', while the other is in right or left slip, indicated by '+' or '−'.

In the four-dimensional space of $(\boldsymbol{x}, \boldsymbol{\lambda}) \in \mathbb{R}^2 \times \mathbb{L}^2$, as the union of the null set of the two functions $g_1(\boldsymbol{x}, \boldsymbol{0}; \boldsymbol{\lambda})$ and $g_2(\boldsymbol{x}, \boldsymbol{0}; \boldsymbol{\lambda})$, the sliding manifold $\mathcal{M}^{ss}$ is a two-dimensional curved surface. It folds over with respect to the λ_i directions (i.e. the coordinate directions λ_i lie in the tangent plane to $\mathcal{M}^{ss}$) along four sets of curves we denote $\mathcal{L}_i^{\pm}$ for $i = 1, 2,$. This folding will be important for the dynamics. It happens where any of the derivatives $\left. \frac{\partial g_i}{\partial \lambda_i} \right|_{\mathcal{M}^{ss}}$ vanish (the derivatives $\frac{\partial g_i}{\partial \lambda_j}$ for $i \neq j$ are identically zero). Solving these conditions $\left. \frac{\partial g_i}{\partial \lambda_i} \right|_{\mathcal{M}^{ss}} = 0$, the curves are found to be given by

$$\mathcal{L}_i^{\pm} = \left\{ (\boldsymbol{x}, \boldsymbol{\lambda}) \in \mathcal{M}^{ss} \; : \; \lambda_i = \lambda^{\pm} \right\}, \tag{23}$$

for $i = 1, 2$, in terms of quantities

$$\lambda^{\pm} = \pm \sqrt{\frac{\mu/\beta + 1}{3}} \,. \tag{24}$$

The portion of $\mathcal{M}^{ss}$ enclosed within the curves $\mathcal{L}_1^{\pm}$ and $\mathcal{L}_2^{\pm}$ we label as

$$\mathcal{M}_a^{ss} = \left\{ (\boldsymbol{x}, \boldsymbol{\lambda}) \in \mathcal{M}^{ss} \; : \; \mu > \beta(3\lambda_i^2 - 1), \; i = 1, 2 \right\} , \tag{25}$$

as depicted in fig. 2.

Lemma 2 (The sliding manifold). $\mathcal{M}_a^{ss} \subset \mathcal{M}^{ss}$ *is an attracting invariant manifold of* (21).

Proof. As stated above, the manifold $\mathcal{M}^{ss}$ consists of the $\boldsymbol{x}$-parameterized family of equilibria of the fast subsystem of (21). The attractivity of these equilibria are described by the Jacobian determinant with respect to the fast subsystem,

$$\left.\frac{\partial \boldsymbol{g}}{\partial \boldsymbol{\lambda}}\right|_{\mathcal{M}^{ss}} = \left.\begin{pmatrix} \frac{\partial g_1}{\partial \lambda_1} & \frac{\partial g_1}{\partial \lambda_2} \\ \frac{\partial g_2}{\partial \lambda_1} & \frac{\partial g_2}{\partial \lambda_2} \end{pmatrix}\right|_{\mathcal{M}^{ss}} = -(\mu + \beta)\begin{pmatrix} 1 & 0 \\ 0 & 1 \end{pmatrix} + 3\beta \left.\begin{pmatrix} \lambda_1^2 & 0 \\ 0 & \lambda_2^2 \end{pmatrix}\right|_{\mathcal{M}^{ss}}, \qquad (26)$$

where Λ_i denotes a root of $g_i(\boldsymbol{x}, \boldsymbol{0}; \boldsymbol{\Lambda}) = \boldsymbol{0}$ where the second row of (21) vanishes, that is

$$0 = -k_i x_i - k_{12}(x_i - x_j) - \rho v - \Lambda_i \mu + \Lambda_i \beta(\Lambda_i^2 - 1), \qquad i = 1, 2. \qquad (27)$$

The Jacobian has eigenvectors $\nu_1 = (1, 0)$, $\nu_2 = (0, 1)$, and eigenvalues $\beta(3\lambda_i^2 - 1) - \mu$. Thus by (25), these eigenvalues are real and negative on $\mathcal{M}_a^{ss}$, hence it is the attracting branch of $\mathcal{M}^{ss}$. □

As the eigenvalues $\beta(3\lambda_i^2 - 1) - \mu$ change sign across the curves $\mathcal{L}_i^{\pm}$ bounding $\mathcal{M}_a^{ss}$, we can see that the attracting branch is surrounded by four repelling regions and four regions of saddle type, as illustrated in fig. 4. Arrows indicate attractivity with respect to the (λ_1, λ_2) fast subsystem, changing where the surface folds along the curves $\mathcal{L}_i^{\pm}$. If we take a two-dimensional cross-section through fig. 4 with $x_1 = x_2 = constant$ we obtain fast phase portraits such as those in fig. 5, cutting $\mathcal{M}^{ss}$ at points P_i and Q_i corresponding to equilibria of the fast (λ_1, λ_2) subsystem.

Considered as an $\boldsymbol{x}$-parameterized family of equilibria of the fast subsystem in $\boldsymbol{\lambda}$ space, the nonlinearity of $\mathcal{M}^{ss}$ implies that, at any $\boldsymbol{x}$, there may exist between 0 and 9 equilibria. These annihilate pairwise in saddlenode bifurcations along the curves $\mathcal{L}_i^{\pm}$. The saddlenode bifurcations (where $\mathcal{M}^{ss}$ folds with respect to the fast directions along $\mathcal{L}_i^{\pm}$) occur at $x_i = X_i^{\pm}(x_j)$, as defined in (28). Codimension two saddlenode bifurcations occur at the points $\mathcal{L}_1^+ \cap \mathcal{L}_2^+$, $\mathcal{L}_1^+ \cap \mathcal{L}_2^-$, $\mathcal{L}_1^- \cap \mathcal{L}_2^+$, $\mathcal{L}_1^- \cap \mathcal{L}_2^-$.

The four points where the curves $\mathcal{L}_i^{\pm}$ intersect are $(x_1, x_2, \lambda_1, \lambda_2) = (X_1^{\pm}, X_2^{\pm}, \lambda^{\pm}, \lambda^{\pm})$, where

$$X_i^{\pm} = -\left(\rho v + \tfrac{2}{3}(\mu + 2\beta)\lambda^{\pm}\right)\frac{k_j + 2k_{12}}{k_1 k_2 + k_{12}(k_1 + k_2)}, \qquad i \neq j. \qquad (28)$$

Our main interest will be on one of the four singularies where the curves $\mathcal{L}_i^{\pm}$ intersect, namely at $Q_* = \mathcal{L}_1^- \cap \mathcal{L}_2^- \in \mathcal{M}^{ss}$ as defined in (20).
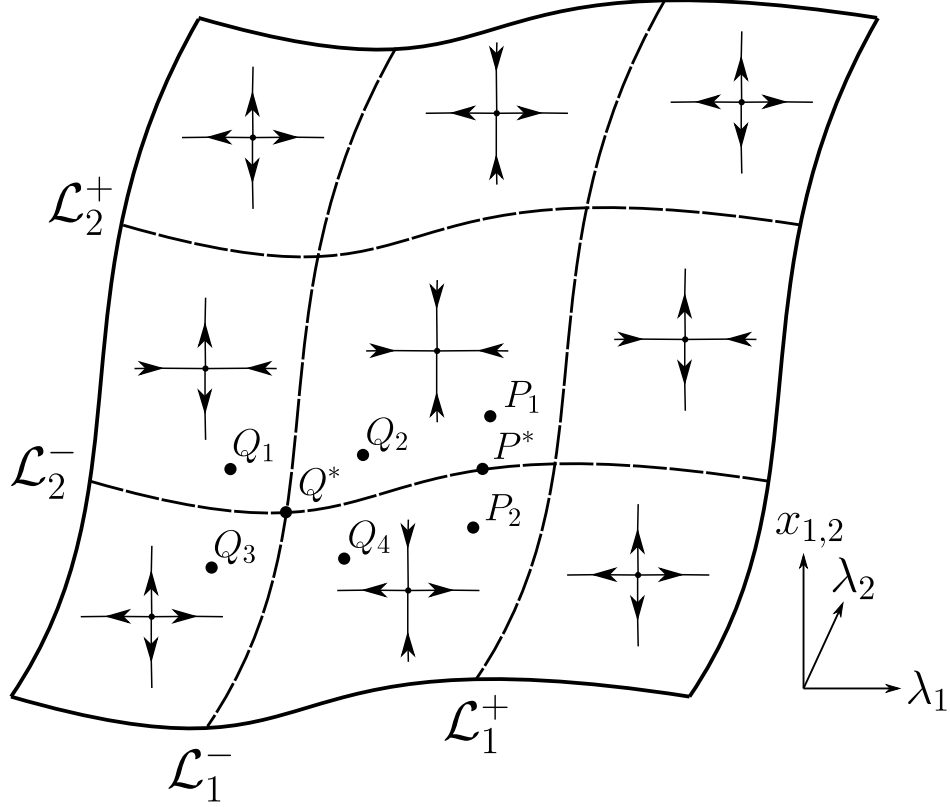
13

Figure 4: The attractivity of the different branches of $\mathcal{M}^{ss}$ (or equivalently of families of equilibria of the fast subsystem on different branches of $\mathcal{M}^{ss}$) with respect to the fast subsystem. This is a representation of dynamics in four dimensions. If we take a two-dimensional section $x_1 = x_2 = constant$, we intersect the surface $\mathcal{M}^{ss}$ at between one and nine points lying in different regions of this figure. Examples are given of sections intersecting at points P1-2, P*, Q1-4, Q*, for which the resulting fast subsystems in the (λ_1, λ_2) plane are shown in fig. 5.
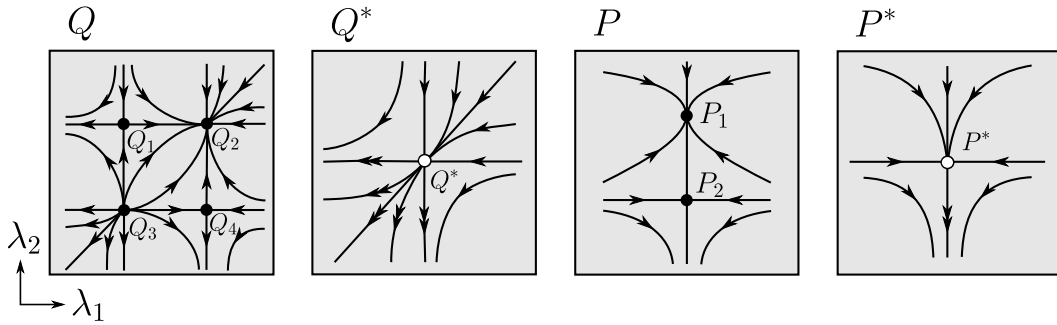

Figure 5: The fast subsystems in the (λ_1, λ_2) plane for cross-sections $x_1, x_2 = constant$, which intersect $\mathcal{M}^{ss}$ at the points P1-2, P*, Q1-4, Q*, shown in fig. 4. The attractors $Q2$ and $P1$ are members of the family of equilibria that make up the attracting branch $\mathcal{M}^{ss}_a$ of $\mathcal{M}^{ss}$.

Lemma 3 (Onset of sliding). *For any curve* $\Gamma \subset \mathcal{M}^{ss}_a$ *there exists a one parameter*

family of orbits of (21) *evolving onto* Γ, *reaching the ε-neighbourhood of* $\mathcal{M}_a^{ss}$ *in a time* $t = \mathcal{O}(\varepsilon \log \varepsilon)$.

Proof. In the neighbourhood of $\mathcal{M}_a^{ss}$, solutions of (21) are given by

$$\lambda_i(t) = \Lambda_i \pm \lambda_i(0) e^{-t\beta(1-3\Lambda_i^2)/\varepsilon} + \mathcal{O}(e^{-2t\beta(1-3\Lambda_i^2)/\varepsilon}) , \tag{29}$$

where Λ_i are the roots of (27), and the term $\beta(1 - 3\Lambda_i^2)$ in the exponent is positive by (25). To find the time taken for the solution to reach an ε-neighbourhood of $\mathcal{M}_a^{ss}$ from a typical point $\lambda_i(0)$ outside $\mathcal{M}_a^{ss}$, we can let $\lambda_i(t) = L_i + \varepsilon$ and solve for t, giving

$$t = -\frac{\varepsilon}{\beta(1 - 3\Lambda_i^2)} \log \frac{\varepsilon}{\lambda_i(0)} = \mathcal{O}(\varepsilon \log \varepsilon) , \tag{30}$$

which vanishes as $\varepsilon \to 0$. Hence on the natural timescale t, solutions inside the switching layer $\hat{\Sigma}_{12}$ collapse onto $\mathcal{M}_a^{ss}$ infinitely fast in the limit $\varepsilon \to 0$.

Since this holds for any point $(x_1, x_2, \Lambda_1, \Lambda_2) \in \mathcal{M}_a^{ss}$, if we take a curve of such points $\Gamma = \{(x_1, x_2, \gamma_1(s), \gamma_2(s)) \in \mathcal{M}_a^{ss} : s \in R \subset \mathbb{R}\}$ parameterized by s on some real interval R, there exists an s-paramerized family of solutions (29) evolving onto Γ in zero time. $\square$

Since the attracting branch $\mathcal{M}_a^{ss}$ is an invariant, solutions can only escape it at its boundaries $\mathcal{L}_i^{\pm}$. Our particular interest is on the escape that occurs at the point $Q* = \mathcal{L}_1^- \cap \mathcal{L}_2^-$ defined in (20).

Lemma 4 (Set-valued exit from the singularity). *The flow exiting Q_* via the fast system* (19) *is set-valued, and departs the ε-neighbourhood of Q_* in finite time, evolving until they reach the boundary of the layer $\hat{\Sigma}_{12}$ with (λ_1, λ_2) values on*

$$\left\{\lambda_1 = -1, \ -1 \leq \lambda_2 \leq \lambda^-\right\} \cup \left\{-1 \leq \lambda_1 \leq \lambda^-, \lambda_2 = -1\right\} .$$

Proof. Introduce local coordinates $\eta_i = \lambda_i - \lambda^-$, so that $\eta_1 = \eta_2 = 0$ at $Q* = \mathcal{L}_1^- \cap \mathcal{L}_2^-$. Subsituting into (21) we have

$$\varepsilon \dot{\eta}_i = 3\beta\lambda^- \eta_i^2 + \beta\eta_i^3 . \tag{31}$$

Note that $\dot{\lambda}_i < 0$ for $\eta_i < -3\lambda^-$. Solutions take the form

$$-\frac{3\lambda^-\beta}{\varepsilon} t = \hat{c} + \frac{1}{\eta_i} + \frac{1}{3\lambda^-} \log\left|1 + \frac{3\lambda^-}{\eta_i}\right| , \tag{32}$$

and we can use this to calculate the time taken to reach the edge of the switching layer from an ε-neighbourhood of $\mathcal{L}_1^- \cap \mathcal{L}_2^-$ as $\varepsilon \to 0$. If we assume a solution starts from

15

$\eta_i = -\varepsilon$ at $t = t_0$, and reaches $\eta_i = -1 - \lambda^-$ (i.e. $\lambda_i = -1$) at $t = t_1$, then from (32), after simplifying, we have

$$t_1 - t_0 = \frac{1 + \lambda^- - \varepsilon}{-3\lambda^- \beta(1 + \lambda^-)} + \frac{\varepsilon}{9(\lambda^-)^2 \beta} \log \left| \frac{1 - \frac{3\lambda^-}{\varepsilon}}{1 - \frac{3\lambda^-}{1 + \lambda^-}} \right|$$

$$= \frac{-1}{3\lambda^- \beta} + \mathcal{O}(\varepsilon) , \tag{33}$$

noting this is positive since $\lambda^- < 0$. Hence solutions reach the switching layer boundary from an ε-neighbourhood of $\eta_1 = \eta_2 = 0$ in finite time as $\varepsilon \to 0$.

We can also look directly at the curves formed by solutions in the (λ_1, λ_2) plane, using (21) to solve

$$\frac{d\eta_2}{d\eta_1} = \frac{\eta_2'}{\eta_1'} = \frac{\eta_2^2(3\lambda^- + \eta_2)}{\eta_1^2(3\lambda^- + \eta_1)}$$

$$\Rightarrow \quad 3\lambda^- \left(\frac{1}{\eta_2} - \frac{1}{\eta_1} \right) = \log \left| \frac{1 + 3\frac{\lambda^-}{\eta_1}}{1 + 3\frac{\lambda^-}{\eta_2}} \right| + const . \tag{34}$$

All solutions pass through $\eta_1 = \eta_2 = 0$, i.e. Q_*, as they must. The slope of the graphs of λ_2 as a function of λ_1 are monotonic, since $d\eta_2/d\eta_1 > 0$ for $\eta_i < 0$ (and moreover for $\eta_i < -3\lambda^-$). Therefore these solutions cannot pass again through the lines $\eta_1 = 0$ or $\eta_2 = 0$ away from $\eta_1 = \eta_2 = 0$, i.e. they cannot pass through $\lambda_i = \lambda^-$ away from $\lambda_1 = \lambda_2 = \lambda^-$, and are confined to the regions $\lambda_i \in [-1, \lambda^-]$. Thus these solutions evolve with decreasing λ_i until they reach $\lambda_1 = -1$ or $\lambda_2 = -1$, whereupon they lie on the layer boundary within $-1 \leq \lambda_1 \leq \lambda^-$ if $\lambda_2 = -1$, or $-1 \leq \lambda_2 \leq \lambda^-$ if $\lambda_1 = -1$. $\quad \square$

We have established that one parameter familes of orbits enter any curve $\Gamma \subset \mathcal{M}_a^{ss}$, reaching it infinitely fast, while the single point Q_* at the corner of $\mathcal{M}_a^{ss}$ is an initial condition for a whole set of orbits exiting to the boundary of the layer it in finite time. Our attention now turns to the dynamics that links these inside $\mathcal{M}_a^{ss}$ itself.

As an aside, another way of describing the geometry of $\mathcal{M}^{ss}$ is as follows. The null sets of the components (g_1, g_2) in the four-dimensional layer define a pair of smooth three-dimensional hypersurfaces $\mathcal{M}_i = \{ (\boldsymbol{x}, \boldsymbol{\lambda}) \in \mathbb{R}^2 \times \mathbb{L}^2 \ : \ g_i(\boldsymbol{x}, 0; \boldsymbol{\lambda}) = 0 \}$ for $i = 1, 2$. These lie transverse to each other, and their intersection $\mathcal{M}^{ss} = \mathcal{M}_1 \cap \mathcal{M}_2$ is a two-dimensional manifold. If each surface $\mathcal{M}_i$ has a (two-dimensional) fold $\mathcal{F}_i = \{ (\boldsymbol{x}, \boldsymbol{\lambda}) \in \mathcal{M}^{ss} \ : \ \frac{\partial g_i}{\partial \lambda_i} = 0 \}$, then this manifests on $\mathcal{M}^{ss}$ as a curve $\mathcal{L}_i = \mathcal{F}_i \cap \mathcal{M}_j$, $i \neq j$, which is a curve where $\mathcal{M}^{ss}$ is tangent to the λ_i-direction. The intersection of folds $\mathcal{L}_1 \cap \mathcal{L}_2 \subset \mathcal{M}^{ss}$ is a point where $\mathcal{M}^{ss}$ is tangent to the x and y directions. In fact each hypersurface $\mathcal{M}_i$ possesses two such folds $\mathcal{F}_i^{\pm}$, giving two folds $\mathcal{L}_i^{\pm} \subset \mathcal{M}^{ss}$ associated with each λ_i direction for $i = 1, 2$, giving four points $\mathcal{L}_1^+ \cap \mathcal{L}_2^+$, $\mathcal{L}_1^+ \cap \mathcal{L}_2^-$, $\mathcal{L}_1^- \cap \mathcal{L}_2^+$, $\mathcal{L}_1^- \cap \mathcal{L}_2^- \subset \mathcal{M}^{ss}$, where the tangent space of $\mathcal{M}^{ss}$ lies in the $\boldsymbol{\lambda}$ coordinate plane.

II The sliding dynamics

Returning to the layer system (19) and letting $\varepsilon \to 0$ gives the system of sliding dynamics

$$\begin{cases} \dot{x}_i = f_i(\boldsymbol{x}, \mathbf{0}; \boldsymbol{\lambda}) & = v \ , \\ 0 = g_i(\boldsymbol{x}, \mathbf{0}; \boldsymbol{\lambda}) & = -k_i x_i - k_{12}(x_i - x_j) - \rho v - \lambda_i \mu + \lambda_i \beta(\lambda_i^2 - 1) \ , \end{cases} \quad (35)$$

for $i = 1, 2$, $j = 2, 1$. The algebraic condition on the second row means this dynamics is constrained to lie on the sliding manifold $\mathcal{M}^{ss}$ defined in (22). The simple flow due to the variation $\dot{x}_i$ is illustrated on $\mathcal{M}_a^{ss}$ in fig. 2.

Our sole concern here is to establish a connection, via this flow, between the fast solutions entering and exiting $\mathcal{M}_a^{ss}$ found in section I. The strictly positive $\dot{x}_i$ imply that sliding trajectories flow away from the curves $\mathcal{L}_i^+$ towards the curves $\mathcal{L}_i^-$. The solutions are easily obtained from (35).

Lemma 5 (Sliding into the singularity). *There exists an orbit Γ on $\mathcal{M}_a^{ss}$, a solution of (35), entering Q_* in finite time.*

Proof. The solutions of the first row of (35) are simply $x_i(t) = x_i(0) + vt$. If we let $x_i(0) = X_i^-$ as defined in (28), and substitute into the second row of (35), we find that solutions on $\mathcal{M}^{ss}$ are given by $(X_1^- + vt, X_2^- + vt, \lambda_1(t), \lambda_2(t))$, where the functions $\lambda_i(t)$ are roots of

$$0 = -k_i(X_i^- + vt) - k_{12}(X_i^- - X_j^-) - \rho v - \lambda_i(t)\mu + \lambda_i(t)\beta(\lambda_i^2(t) - 1) \ . \quad (36)$$

Using the definition of X_i^- from (28) this re-arranges to

$$(1 + \tfrac{\mu}{\beta})\lambda_i(t) - \lambda_i^3(t) = (1 + \tfrac{\mu}{\beta})\left(\lambda^- - k_i vt\right) - (\lambda^-)^3 \ . \quad (37)$$

Let Γ be the t-parameterized curve

$$\left\{ (X_1^- + vt, X_2^- + vt, \lambda_1(t), \lambda_2(t)) \ : \ t \in [-T, 0] \right\}$$

for some $T > 0$, where the functions $\lambda_1(s)$ are the roots of (37). At $t = 0$ the equation (37) implies $\lambda_i(t) = \lambda^-$, hence the solution passes through Q_* at $t = 0$, and reaches it in finite time from any point on Γ. $\qquad\square$

4.B Layer systems on Σ_1 or Σ_2 (for one block sticking)

The set Σ_{12}, which we blew up above, is the intersection of the two discontinuity surfaces Σ_1 and Σ_2, on which block 1 and block 2 stick to the surface, respectively. We have to blow up these surfaces separately.

On Σ_1, where $y_1 = 0$, we substitute $y_1 = \varepsilon \lambda_1$ for $\lambda_1 \in \mathbb{L}$ into (15), to obtain

$$
\begin{cases}
\dot{\boldsymbol{x}} & = \boldsymbol{f}(\boldsymbol{x}, (0, y_2); \boldsymbol{\lambda}) \, , \\
\varepsilon \dot{\lambda}_1 & = g_1(\boldsymbol{x}, (0, y_2); \boldsymbol{\lambda}) \, , \\
\dot{y}_2 & = g_2(\boldsymbol{x}, (0, y_2); \boldsymbol{\lambda}) \, ,
\end{cases}
\tag{38}
$$

where $\lambda_1 = \operatorname{sign} y_1$, to be considered for $\varepsilon \to 0$, on the layer

$$
\hat{\Sigma}_1 = \left\{ (\boldsymbol{x}, y_1, \lambda_2) \in \mathbb{R}^2 \times \mathbb{R} \times \mathbb{L} \right\} \, .
$$

On Σ_2, where $y_2 = 0$, we substitute $y_2 = \varepsilon \lambda_2$ for $\lambda_2 \in \mathbb{L}$ into (15), to obtain

$$
\begin{cases}
\dot{\boldsymbol{x}} & = \boldsymbol{f}(\boldsymbol{x}, (y_1, 0); \boldsymbol{\lambda}) \, , \\
\dot{y}_1 & = g_1(\boldsymbol{x}, (y_1, 0); \boldsymbol{\lambda}) \, , \\
\varepsilon \dot{\lambda}_2 & = g_2(\boldsymbol{x}, (y_1, 0); \boldsymbol{\lambda}) \, .
\end{cases}
\tag{39}
$$

where $\lambda_1 = \operatorname{sign} y_1$, to be considered for $\varepsilon \to 0$, on the layer

$$
\hat{\Sigma}_2 = \left\{ (\boldsymbol{x}, \lambda_1, y_2) \in \mathbb{R}^2 \times \mathbb{L} \times \mathbb{R} \right\} \, .
$$

In both cases we omit terms of order ε on the righthand side as they have no significance when we take $\varepsilon \to 0$.

The analysis of this system proceeds following section 2 similar to that above. The simple outcome is that each layer possesses familes of equilibria of the one-dimensional fast subsystems on λ_i. These form three-dimensional sliding manifolds inside each layer. On Σ_1 this sliding manifold is given by

$$
\mathcal{M}^{s\pm} = \left\{ (\boldsymbol{x}, y_1, \lambda_2) \in \mathbb{R}^2 \times \mathbb{R} \times \mathbb{L} \ : \ g_1(\boldsymbol{x}, (0, y_2); \lambda_1, \pm 1) = 0 \right\}
\tag{40}
$$

for $y_2 \gtrless 0$. On Σ_2 the sliding manifold is given by

$$
\mathcal{M}^{\pm s} = \left\{ (\boldsymbol{x}, \lambda_1, y_2) \in \mathbb{R}^2 \times \mathbb{L} \times \mathbb{R} \ : \ g_2(\boldsymbol{x}, (y_1, 0); \pm 1, \lambda_2) = 0 \right\}
\tag{41}
$$

for $y_1 \gtrless 0$.

Since the equations $g_i = 0$ are cubic expressions in the λ_i, the manifolds $\mathcal{M}^{s\pm}$ and $\mathcal{M}^{\pm s}$ are cubic surfaces (in the sense that the surface where $g_i = 0$ is a developable surface whose cross-section in the $(x_1, y_{j \neq i})$ or $(x_2, y_{j \neq i})$ planes is a cubic curve). Each has a branch in $\lambda^- < \lambda_i < \lambda^+$ that is attracting with respect to the appropriate fast λ_i subsystem from (38) or (39) in the limit $\varepsilon \to 0$, lying between repelling branches. This attractivity is verified by considering the derivatives along the fast flows, $\partial g_i / \partial \lambda_i = -\mu - \beta + 3\beta \lambda_i^2$ where λ_i is a solution of $g_i = 0$ as in (40) or (41). At $\lambda_i = \lambda^\pm$ these derivatives vanish, so the equilibria on these manifolds undergo saddlenode bifurcations.

18

Substituting $\lambda_i = \lambda^-$ into $g_i = 0$ shows that these saddlenodes occurs on $\mathcal{M}^{s\pm}$ at $x_1 = X_1^{\pm}$ and on $\mathcal{M}^{\pm s}$ at $x_2 = X_2^{\pm}$. These saddlenode bifurcations correspond to a folding of the manifolds $\mathcal{M}^{s\pm}$ and $\mathcal{M}^{\pm s}$ considered as surfaces in their respective layers.

Using these elements we can ask what happens to solutions that enter these layers $\hat{\Sigma}_1$ and $\hat{\Sigma}_2$, after they have left the the intersection layer $\hat{\Sigma}_{12}$.

Lemma 6 (Re-collapse of solutions). *Solutions entering the layer $\hat{\Sigma}_1$ or $\hat{\Sigma}_2$ at*

$$(x_1, x_2, y_1, y_2) = (X_1^-, X_2^-, 0, 0) \,,$$

with λ_i values on the set

$$\left\{\lambda_1 = -1, \ -1 \le \lambda_2 \le \lambda^-\right\} \cup \left\{-1 \le \lambda_1 \le \lambda^-, \lambda_2 = -1\right\} \,,$$

collapse to $(\lambda_1, \lambda_2) \in [-1, -1]^2 + \mathcal{O}(\varepsilon)$ while remaining within $x_i = X_i^- + \mathcal{O}(\varepsilon)$, prior to exiting the layer into the region $y_1, y_2 < 0$.

Proof. Consider an initial condition on Σ_1 at the intersection Σ_{12}, i.e. $y_1 = y_2 = 0$, with $\lambda_1 \in [-1, \lambda^-]$ and $\lambda_2 = -1$. Let us find how this evolves into the layer $\hat{\Sigma}_1$, i.e. into $y_2 < 0$ with $\lambda_2 = -1$ fixed, through the system (38).

The dynamics encountered inside Σ_1 also depends on the initial conditions of x_1, x_2, and we are interested only in $x_i = X_i^-$ for $i = 1, 2,$, with X_i^- defined in (28). At these coordinates the sliding manifold $\mathcal{M}^{s-}$ has a fold, since $\partial g_1 / \partial \lambda_1 = 0$ on $g_1 = 0$, meaning that the fast subsystem contains a saddlenode, and (38) becomes

$$
\begin{cases}
\dot{x}_1 & = v \,, \\
\dot{x}_2 & = y_2 + v \,, \\
\varepsilon \dot{\lambda}_1 & = \beta(\lambda^- - \lambda_1)^2(2\lambda^- + \lambda_1) + \mathcal{O}(x_1 - X_1^-, x_2 - X_2^-) \,, \\
\dot{y}_2 & = \beta(\lambda^- + 1)^2(2\lambda^- - 1) + \mathcal{O}(x_1 - X_1^-, x_2 - X_2^-) \,,
\end{cases}
\tag{42}
$$

Note that using the defintion of λ^- from (24), and the fact that $\lambda_1 \le 1$, we have $2\lambda^- + \lambda_1 \le -2\frac{\mu+\beta}{3\beta} + 1 < -2/\sqrt{3} + 1 < 0$. Hence $\dot{\lambda}_1$ is strictly negative, and therefore λ_1 evolves from the initial condition $\lambda_1(0) \in [-1, \lambda^-]$ to the boundary of the layer $\hat{\Sigma}_1$ at $\lambda_1(t) = -1$ in a time $t = \mathcal{O}(\varepsilon)$. Re-scaling to the fast time t/ε the system becomes

$$
\begin{cases}
x_1' & = \mathcal{O}(\varepsilon) \,, \\
x_2' & = \mathcal{O}(\varepsilon) \,, \\
\lambda_1' & = \beta(\lambda^- - \lambda_1)^2(2\lambda^- + \lambda_1) + \mathcal{O}(\varepsilon) \,, \\
y_2' & = \mathcal{O}(\varepsilon) \,,
\end{cases}
\tag{43}
$$

therefore the x_i variables will vary as $x_i - X_i^- = \mathcal{O}(\varepsilon)$. The result for the similar collapse of solutions in the layer $\hat{\Sigma}_2$ follows simply by switching labels $1 \leftrightarrow 2$ in the arguments above. $\qquad \square$

This implies that λ_1 will evolve from any initial condition on $\lambda_1 \in [-1, \lambda^-)$ to $\lambda_1 = -1$ in the time $t = \mathcal{O}(\varepsilon)$, while x_1, x_2, y_2, change by only $\mathcal{O}(\varepsilon)$. (The time taken to evolve from $\lambda_1 \in [\lambda^-, +1]$ to $\lambda_1 = -1$ will be longer and x_1, x_2, y_2, would vary more, but we will not need to consider this region).

Having reached the boundary of the switching layer on Σ_1, the flow must exit into $y_1, y_2 < 0$, and will evidently do so with $y_1 = 0$, $y_2 = \mathcal{O}(\varepsilon)$.

A corresponding analysis describes exit from the intersection Σ_{12} to the surface Σ_2, culminating in exit into $y_1, y_2 < 0$, with coordinates $y_1 = \mathcal{O}(\varepsilon)$, $y_2 = 0$.

4.C   Micro-indeterminacy

Proposition 1 follows by putting together lemma 2 to lemma 5, with part 1 given by lemma 2, 3, & 5, part 2 given by lemma 4, and part 3 given by lemma 6. To describe this more explicitly we put the dynamics derived of the two oscillators in section 4 together, concatening the flows of various t and t/ε timescale subsystems.

Firstly lemma 2 tells us that the manifold $\mathcal{M}_a^{ss}$, which corresponds to both blocks in sticking motion, is an attractor. Lemma 3 tells us that any curve Γ on $\mathcal{M}_a^{ss}$ is reached by a one parameter family of orbits in finite time (including infinitely fast contraction through the fast layer flow). A typical trajectory through $\mathcal{M}_a^{ss}$ will eventually exit the sliding manifold (i.e. the sticking state) through one of the folds $\mathcal{L}_1^-$ or $\mathcal{L}_2^-$, from which either block 1 or block 2 begins slipping respectively. Figure 6 illustrates such a trajectory evolving along $\mathcal{M}^{ss}$ and exiting along a fold; sections through $\mathcal{M}^{ss}$ are shown illustrating the fast flow in which $\mathcal{M}^{ss}$ appears as a family of equilibria.

In lemma 5 we identify the curve Γ with a sliding trajectory that enters the singualrity Q_* in finite time. This is in effect a separatrix between those solutions that exit along $\mathcal{L}_1^-$ and $\mathcal{L}_2^-$. Lemma 4 shows that this trajectory, which is deterministic until Q_*, then explodes into a multi-valued set from which one block after another will slip, in an indeterminable sequence. This is illustrated in fig. 7, showing a solution Γ traveling along $\mathcal{M}_a^{ss}$ into Q_*, where the folds of the two null sets $g_1 = 0$ and $g_2 = 0$ coincide. (The manifold $\mathcal{M}^{ss}$ is the intersection of these null sets $g_1 = g_2 = 0$, and further solutions are pictured along these intersection, but these lie on regions where $\mathcal{M}^{ss}$ is not an attractor but is saddle-like or repelling with respect to the fast flow). Exit then occurs via the fast flow.

This indeterminacy of the block's exit from sticking is concerning in a mechanical system, but lemma 6 then shows that the dynamics conspires to hide it, collapsing solutions back down to an $\mathcal{O}(\varepsilon) \to 0$ set of conditions in which both blocks slip.
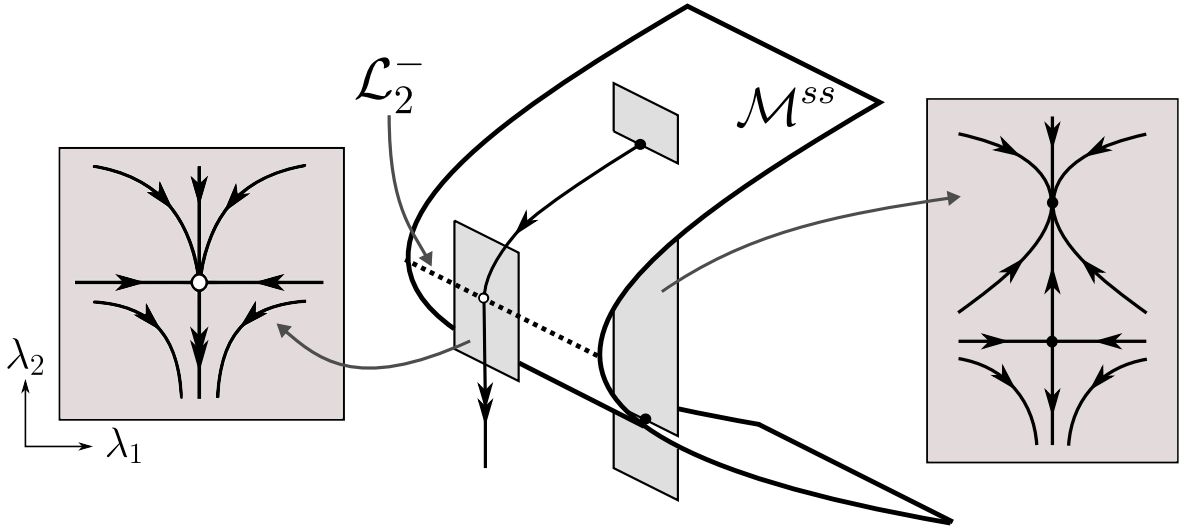
Figure 6: The manifold $\mathcal{M}^{ss}$ in the vicinity of $\mathcal{L}_2^-$, showing entry to the fold $\mathcal{L}_2^-$ through the sliding flow, followed by exit through the fast flow. This is a schematic representation of the two-dimensional manifold $\mathcal{M}^{ss}$ in the four dimensional space of $(x_1, x_2, \lambda_1, \lambda_2)$. Sections through the manifolds are shown, illustrating the phase portrait of the fast flow; in the right portrait the intersection with $\mathcal{M}^{ss}$ corresponds to an attracting node and a saddle; on the fold these have come together in a fold bifurcation shown in the left portrait. The flow is deterministic.
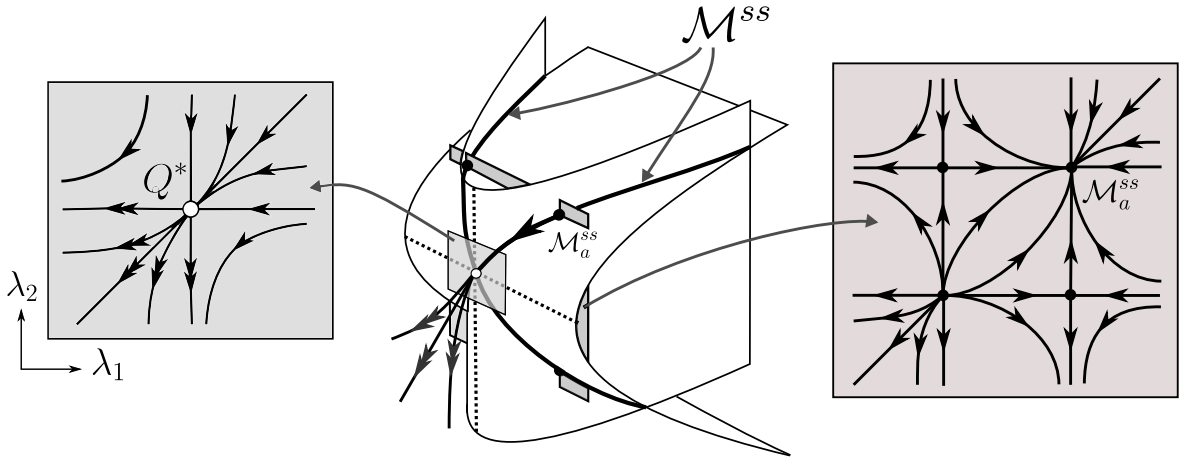

Figure 7: The corresponding piecture to fig. 6 in the vacinity of $Q_* = \mathcal{L}_1^- \cap \mathcal{L}_2^-$. Here we choose a different schematic representation of the four dimensional space of $(x_1, x_2, \lambda_1, \lambda_2)$, illustrating that $\mathcal{M}^{ss}$ is the intersection of the null sets $g_1 = 0$ and $g_2 = 0$ (the two parabolic surfaces). The point $Q_* = \mathcal{L}_1^- \cap \mathcal{L}_2^-$ lies where the folds of the null sets coincide. Sliding solutions on $\mathcal{M}^{ss}$ are shown, including a trajectory entering the singularity along $\mathcal{M}_a^{ss}$, and exiting through the fast flow. Sections through $\mathcal{M}^{ss}$ show the phase portrait of the fast flow, where $\mathcal{M}^{ss}$ corresponds to four equilibria, which collide at the singularity.

What we will show in the following section is that this fleeting loss of determinacy

nevertheless has global consequences. We will also show in lemma 7 that this is not a peculiarity of the nonsmooth model or of taking the limit $\varepsilon \to 0$, but persists for $\varepsilon > 0$ and if we smooth out the system's discontinuities.

The detailed analysis above resolves a potential ambiguity if one analyses the system only on the timescale t. In doing so one would first calculate the slipping dynamics (outside Σ_1 and Σ_2) and the sliding dynamics (on $\mathcal{M}^{s\pm}$ in Σ_1, on $\mathcal{M}^{\pm s}$ in Σ_2, and on $\mathcal{M}^{ss}$ in Σ_{12}). This would reveal places where it is impossible to decide whether one or both blocks will slip, or in what sequence they do so.

Analysis of the fast dynamics inside the layers reveals that for typical initial conditions, one block alone slips and this can be determined uniquely (the scenario of exit via a fold in fig. 6). For one isolated initial condition the system will evolve through the point $\mathcal{L}_1^- \cap \mathcal{L}_2^-$ from which the onward evolution is non-deterministic, something not regularly encountered in a typical mechanical problem. Surprisingly, however, the fast dynamics conspires to conceal that determinacy breaking. The onward evolution consists almost entirely of solutions in which the blocks both ultimately slip via some sequence, one very quickly (at time $t = \mathcal{O}(\varepsilon)$ after the other), and via a definite sequence, the alternate phase space trajectories squashed to within an ε-small region of phase space.

5   Simulations and singular perturbation

We can illustrate the global significance of the microscopic indeterminacy described above with simulations of the full system's dynamics. A choice must be made about how to simulate the piecewise-smooth dynamics, given that it contains both discontinuity (which could be handled using event detection), and loss of determinacy (which cannot).

The most complete way to simulate the oscillator is to calculate the set of all possible forward motions whenever a loss of determinacy is detected, but we have studied these sufficiently with the analysis above. Instead we wish to understand the practical significance of the phenomenon in the less idealized conditions found in applications, or in a 'regularized' formulation of (15) that seeks to restore determinacy. Regularization is commonly used in contact problems, introducing compliance of the rigid body in applications (see [11, 25, 32] for recent examples). It is also commonly used as analytical approach to discontinuities, replacing the discontinuous quantities λ_i with smooth functions analyzable with singular perturbation methods (see [39, 50] for key principles).

Smooth models obtained by regularization are still highly idealized from an applied point of view, and from an applied point of view it is important to consider the effect

of more irregular perturbations, from environmental conditions such as machine vibra-
tions or irregularity of the contact surface (see e.g. [37, 43, 5]). Again these are also of
major interest in the perturbative study of nonsmooth systems (e.g. [49, 31, 48]). The
indeterminacy at Q_* represents an extreme sensitivity of the flow to initial conditions
or fluctuations in the vector field, so such irregular perturbations are highly relevant.

To this end we will regularize the oscillator system by both smoothing the discontinuity
and adding small random perturbations simulating noise.

An important observation, and a potentially surprising one given the high codimension
of the singularity concerned, is that the micro-indeterminacy phenomenon survives
regularization to a smooth system.

Consider regularizing by replacing $\lambda_i \mapsto \phi_i(y_i/\varepsilon)$ in (19) for $i = 1, 2$, where ϕ_i are
smoothly differentiable monotonic functions satisfying

$$\phi_i(y/\varepsilon) = \text{sign}(y) + \mathcal{O}(\varepsilon) \quad \text{if} \quad |y| \geq \varepsilon . \tag{44}$$

Substituting these directly into the system (15) on $y_1 = y_2 = 0$, and letting $u_i = y_i/\varepsilon$,
gives

$$\begin{cases} \dot{x}_i & = f_i(\boldsymbol{x}, \boldsymbol{y}; \phi_1(u_1), \phi_2(u_2)) \\ & = \varepsilon u_i + v , \\ \varepsilon \dot{u}_i & = g_i(\boldsymbol{x}, \boldsymbol{y}; \phi_1(u_1), \phi_2(u_2)) \\ & = -k_i x_i - k_{12}(x_i - x_j) - \rho v - (\mu + \beta)\phi_i(u_i) + \beta\phi_i^3(u_i) . \end{cases} \tag{45}$$

The proper treatment of this is then by singular perturbation analysis (see e.g. [18,
33, 50] for standard methods). In short, for $\varepsilon \to 0$ this two-timescale system possesses
a critical manifold $\mathcal{M}$ where $g_1 = g_2 = 0$, which is equivalent to the sliding manifold
$\mathcal{M}^{ss}$, and for $\varepsilon > 0$ there exist invariant manifolds in the ε-neighbourhood of points
where the critical manifold $\mathcal{M}$ is normally hyperbolic with respect the fast (u_1, u_2)
subsystem. Clearly, given the similarity of the righthand sides of (15) and (45), there
exists a singularity Q_*^ε where $g_1 = g_2 = 0$ and $\frac{\partial g_1}{\partial u_1} = \frac{\partial g_2}{\partial u_2} = 0$, analogous to the point
Q_* in the nonsmooth system.

Typically the study of such singularities under perturbation to $\varepsilon > 0$ is highly non-
trivial (see e.g. the singular perturbation of folds of critical manifolds [53] or the
regularization of the two-fold singularity in nonsmooth systems [29, 51]), due mainly to
the lack of explicit expressions for, and potential complexity of, the invariant manifolds
for $\varepsilon > 0$.

In this case, however, the situation is rather more simple, as the phenomenon does not
depend on the precise form of the invariant manifolds in the ε-neighbourhood of $\mathcal{M}$,
but on the existence of the deterministic in-flow, and set-valued out-flow, through Q_*
as established in proposition 1 and lemma 2 to 5.

Lemma 7 (Persistence under perturbation). *The micro-indeterminacy described in proposition 1, through the determinacy-breaking singularity Q_* in the layer system (19), persists in the smoothed system (45) for $\varepsilon > 0$.*

Proof. To show this we need only look at what happens close to the singularity Q_*. We begin by comparing the local expression for the layer dynamics (19) around Q_* in the nonsmooth system, with a similar expression derived from the smoothed system (45).

First, in the nonsmooth system, take local coordinates $\xi_i = x_i - X_i^-$ and $\eta_i = \lambda_i - \lambda^-$, in terms of which (19) on $\hat{\Sigma}_{12}$ becomes

$$\begin{cases} \dot{x}_i = f_i(\boldsymbol{x}, \boldsymbol{0}; \boldsymbol{\lambda}) &= v \, , \\ \varepsilon \dot{\eta}_i = g_i(\boldsymbol{x}, \boldsymbol{0}; \boldsymbol{\lambda}) &= K(\xi_i, \xi_j) - 3\beta\eta_i^2 + \mathcal{O}(\eta_i^3) \, , \end{cases} \tag{46}$$

where $K(\xi_i, \xi_j) = -k_i \xi_i - k_{12}(\xi_i - \xi_j)$, $i \neq j$.

Now take the smoothed system (45), and define a point Q_*^ε with coordinates $(x_1, x_2, u_1, u_2) = (X_1^-, X_2^-, u_1^-, u_2^-)$, where X_i^- are as defined in (28), and u_i^- are the solutions of

$$\phi_i(u_i^-) = -\sqrt{\frac{\mu + \beta}{3\beta}} \, . \tag{47}$$

Expanding (45) about Q_*^ε, by letting $w_i = u_i - u^-$ and expanding $\phi_i(u_i) = \phi_i(u_i^-) + w_i \phi_i'(u_i) + \frac{1}{2} w_i^2 \phi_i''(u_i) + ...$, gives

$$\begin{cases} \dot{x}_i = f_i(\boldsymbol{x}, \boldsymbol{y}; \phi_1(u_1), \phi_2(u_2)) &= v + \mathcal{O}(\varepsilon) \, , \\ \varepsilon \dot{u}_i = g_i(\boldsymbol{x}, \boldsymbol{y}; \phi_1(u_1), \phi_2(u_2)) &= K(\xi_i, \xi_j) - 3Bw_i^2 + \mathcal{O}(w_i^3, \varepsilon) \, , \end{cases} \tag{48}$$

where we have made use of (28) and (47), and the constant B is

$$B = \beta \left\{ \frac{1}{2}(\lambda^-)^2 \phi_i''(u_i) + \phi_i(u_i^-)\phi_i'(u_i)^2 + \frac{1}{2}\phi_i(u_i^-)^2 \phi_i''(u_i) \right\} \, . \tag{49}$$

This is equivalent to (46) to higher order terms.

Hence the smoothed system (45) exhibits the same local singularity, with a topologically equivalent fast subsystem, to that of the nonsmooth system's layer dynamics (15). Lemma 4 applies directly to (45) by substituting (λ_1, λ_2) with (u_1, u_2): there exists a singularity Q_*^ε where $g_1 = g_2 = 0$ and $\frac{\partial g_1}{\partial u_1} = \frac{\partial g_2}{\partial u_2} = 0$ (immediately obvious from the local expression (48)), from which the exit is indeterminate — a set-valued flow filling the region $u_1, u_2 \leq 0$.

It remains to show that there still exists a solution of the smooth system that enters the singularity. This is guaranteed by the slow dynamics, $\dot{x}_i \approx v_i$, being constant and

24

non-vanishing to leading order. Hence in the smooth system there exist trajectories

$$(x_1(t), x_2(t), x_3(t), u_1(t), u_2(t)) = (v_1 t, v_2 t, v_3 t, u_1^*(t), u_2^*(t)) + \mathcal{O}(t^2)$$

where u_i^* are functions such that

$$g_i(v_1 t, v_2 t, v_3 t, \phi_1(u_1^*(t)), \phi_2(u_2^*(t))) = 0$$

for $i = 1, 2$, and at $t = 0$ by the definition of g_i in (45) these lie at the singularity Q_*^ε. $\qquad\square$

A corresponding result determining what happens to the local dynamics under irregular perturbations, for example adding random noise, would require substantially more intricate analysis involving stochastic partial differential equations, studying the probability density function of solutions near the singularity and mean exits times from its vacinity. We omit such lengthy analysis here and turn directly to simulations.

To simulate the oscillator we first smooth its discontinuous terms, replacing each switching multiplier λ_i with a smooth sigmoid function $\phi^\varepsilon(y_i)$ satisfying (44). For the purpose of these simulations we take $\phi_\varepsilon(y_i) = \tanh(y_i/\varepsilon)$ and $\varepsilon = 10^{-3}$. By virtue of the theorem above and results in [39], the exact choice of ϕ does not significantly affect the results provided it is monotonic and tends to $\text{sign}(y_i)$ for $\varepsilon \to 0$. We then simulate the effect of noise by adding random perturbations to the system's state at small time increments.

In the oscillator model from section 4, the two blocks exhibit quasi-periodic stick-slip motion that repeatedly carries them close to the determinacy-breaking singularity. That is, solutions make repeated excursion through the regions $y_1 < 0$ and $y_2 < 0$ (corresponding to leftward slip of the block relative to the frictional surface), interrupted by intervals of sliding along $y_1 = 0$ and/or $y_2 = 0$ (corresponding to block 1 and/or 2 sticking to the surface). Although the singularity itself has zero measure, its effect on nearby trajectories has a mixing effect on the global dynamics of the system.

Three simulations for the same set of parameters and initial conditions (see caption) are plotted in fig. 8. The right-hand panels show the oscillations of blocks 1 and 2 in their respective phase planes. The left-hand plots show trajectories passing through the neighbourhood of the singularity in the velocity plane.

The effect of the singularity is seen in the creation of bistability between two attractors, namely the largest and smallest limit cycles seen in the right-hand panels of fig. 8. Before settling to one of these attractors the blocks may wander towards one or other attractor, as in A and C, or tend more simply towards just one attractor as in B. These behaviours are indicated by the shading. The gradient from red to blue signifies the passing of time, and the first few returns are also labelled to indicate the early wandering of the solutions on successive returns.
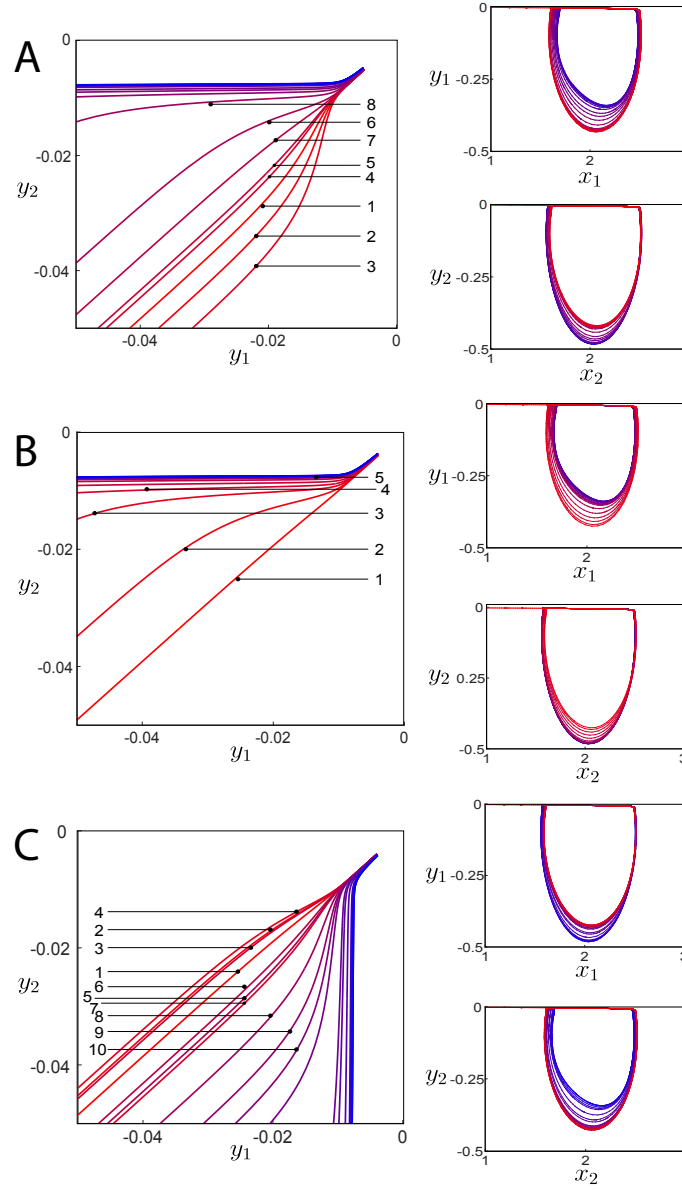
25

Figure 8: A-C: Three simulated trajectories of the oscillator system (15), each shown in three different coordinate planes. The colour gradient represents the time dimension, with red at time $t = 0$, and blue at the end of the simulation. On the left is the (y_1, y_2)-plane at a scale where the dynamics on the discontinuities is visible inside $y_{1,2} \in [-\varepsilon, +\varepsilon]$. On the right is the phaseplane for either block, block one above and block two below. Cases A, B and C all have identical initial conditions $(x) = (-1, -1)$, $\boldsymbol{y} = (0, 0)$ and parameter values $\varepsilon = 0.01$, $k_1 = 0.5$, $k_2 = 0.5$, $k_{12} = 0.4$, $\rho = 0.1$, $v = 0.1$, $\mu = 1$, $\beta = 1.5$.

Thus the local instability around the singularity manifests itself in the mixing of the basins of attraction of the limit cycles seen in the right of fig. 8. While wandering between these basins, as seen in the left of fig. 8, the instability also manifests locally

as the velocity profiles explore a set of values induced by the set-valued exit from the singularity.

The local instability of the singularity also manifests itself locally in the friction force F_i acting on each block near their exit from sticking. By plotting the ratio of these friction forces near the slipping point for simulation C in fig. 9 we can see how the friction force on each block varies on an order much larger than ε, as solutions pass close to the singularity.
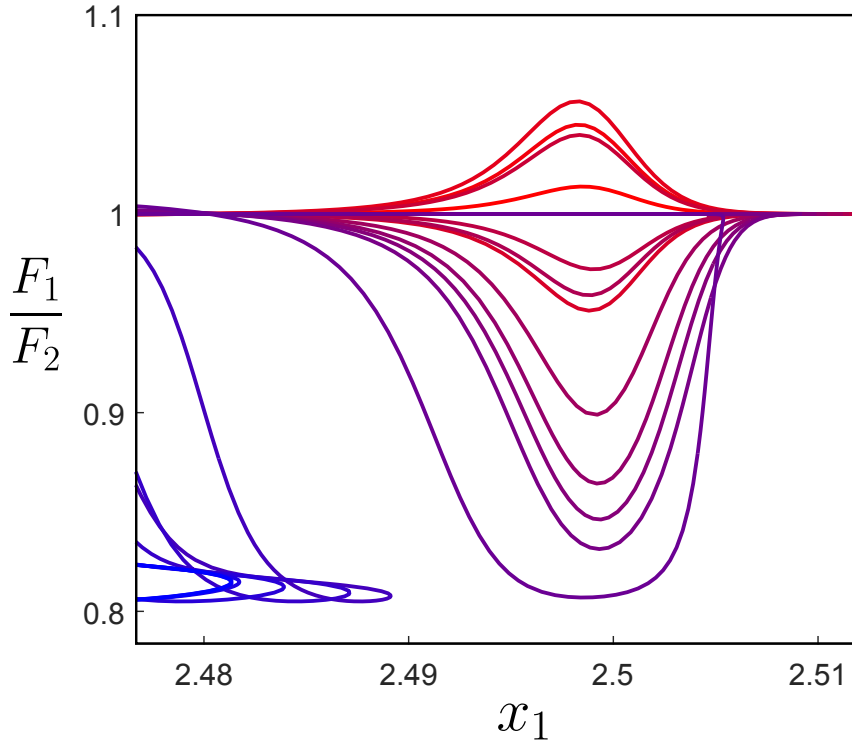

Figure 9: The ratio of friction forces acting on each block near the singularity. The figure is generated using the trajectory from simulation C in fig. 8.

Without noise in these simulations we see (in simulations not shown) less transitivity, that is, a tendency to travel more uniformly towards on limit cycle, as seen in B. This is instructive about what is happening in simulations A-C in fig. 8. Solutions pass close to the singularity upon exit and are then split apart by the local (non-deterministic) intability towards one or other attractor. The basins of the attractors are such that in a smooth system they remain distinct, and the ultimate attractor is determined by initial conditions, but the basins are sufficiently entwined that very small noise makes their boundaries indistinct, and solutions are able to wander between the two, until at late times when a solution has converged close enough to a limit cycle to be trapped inside one basin or the other.

6 Perturbation from the decoupled case

The micro-scale determinacy-breaking described above takes a particularly simple form because the discontinuous terms of the two oscillators are decoupled, namely $\dot{x}_i$ depends only on λ_i and not on $\lambda_{j \neq i}$. The phenomenon can occur more generally if such coupling terms do appear, and turns out then to have more severe global consequences, with the breakdown in determinacy no longer being confined to an ε-neighbourhood.

The model (19) satisfies the local conditions of the singularity, namely

$$\dot{\lambda}_1 = \dot{\lambda}_2 = \frac{\partial \dot{\lambda}_1}{\partial \lambda_1} = \frac{\partial \dot{\lambda}_2}{\partial \lambda_2} = 0 \, , \qquad \frac{\partial^2 \dot{\lambda}_1}{\partial \lambda_1^2}, \; \frac{\partial^2 \dot{\lambda}_2}{\partial \lambda_2^2} \neq 0 \, , \tag{50}$$

while possessing a decoupling that expresses the independence of the oscillator's friction forces

$$\frac{\partial \dot{\lambda}_1}{\partial \lambda_2} = \frac{\partial \dot{\lambda}_2}{\partial \lambda_1} = 0 \, . \tag{51}$$

To obtain a more general form where such coupling does occur we need only introduce a perturbation that breaks this degeneracy. A mixed linear term is sufficient, that is, perturbing (15) such that the friction forces of the blocks are coupled, writing

$$F(\lambda_i, \lambda_j) = \lambda_j \tilde{\mu} - \lambda_i \mu - \lambda_i \beta(\lambda_i^2 - 1) \, , \tag{52}$$

via some coupling coefficient $\tilde{\mu}$, in the system

$$\begin{cases} \dot{x}_i = f_i(\boldsymbol{x}, \boldsymbol{y}; \boldsymbol{\lambda}) & = y_i + v \, , \\ \dot{y}_i = g_i(\boldsymbol{x}, \boldsymbol{y}; \boldsymbol{\lambda}) & = -k_i x_i - k_{12}(x_i - x_j) - \rho(y_i + v) - F(\lambda_i, \lambda_j) \, , \end{cases} \tag{53}$$

for $i = 1, 2$, $j = 2, 1$, as before, with $\boldsymbol{\lambda} = (\lambda_1, \lambda_2)$ and $\lambda_i = \text{sign}(y_i)$. We recover the simple oscillator for $\tilde{\mu} = 0$.

We will only give a brief outline of the effect of this perturbation, leaving its analysis to future work. We omit a detalied study because this system desrves substantial further consideration, of the physical meaning of this perturbation both in the mechanical context and to wider applications, and of the implications of the singularity in the wider context of multiple-timescale systems and singular perturbations.

The fast flows of (15) and (53) near Q_* are plotted in fig. 10. These show the flow exiting from Q_*. In the case of the oscillator the flow fills the lower left quadrant of the fast subsystem's phase space, $\lambda_1, \lambda_2 < \lambda^-$ (η_1, η_2 in the local coordinates around Q_*), in the perturbed case filling a larger region in the left half-plane $\lambda_1 < \lambda^-$ ($\eta_1 < 0$ in the local coordinates).
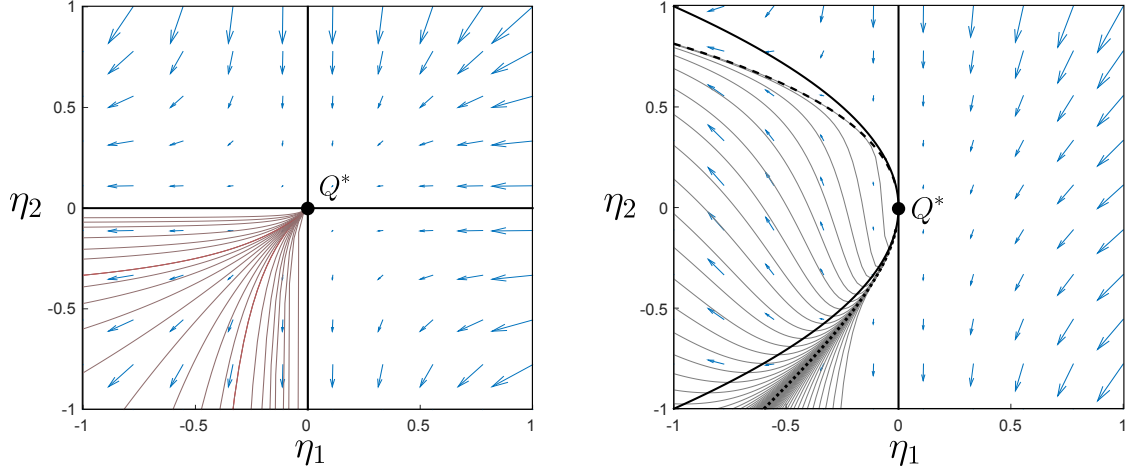
Figure 10: Plot of the fast subsystem in the layer $\hat{\Sigma}_{12}$, in the oscillator (left) and the generic perturbation (right), showing the local flow field, and a number of solutions exiting the origin. Plotted in local coordinates $\eta_i = \lambda_i - \lambda^-$ about the singuarity Q_*.
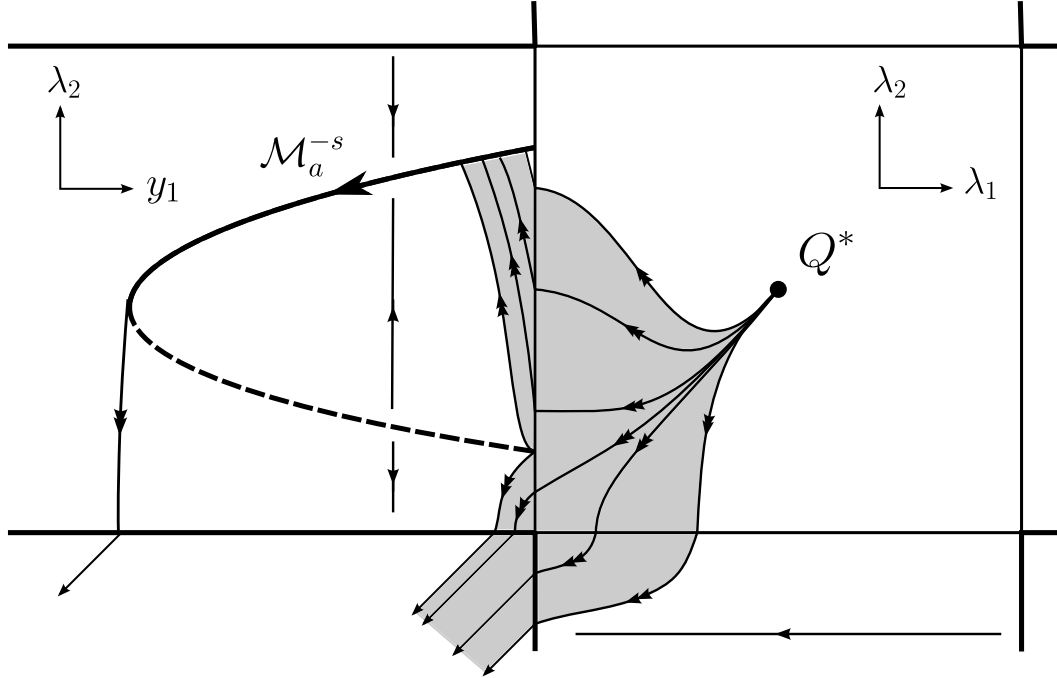

Figure 11: A sketch of the system (53) taking a cross-section through constant x, schematically showing the set-valued exit from Q_* inside the layer $\hat{\Sigma}_{12}$, entering the layer $\hat{\Sigma}_2$ and splitting into a lower stream of solutions that go directly to slip, and an upper stream of solutions that slide along $\mathcal{M}_a^{-s}$ (corresponding to block 2 sticking) which block 1 slips.

The effect on the overall flow, and on micro-indeterminacy, is sketched in fig. 11. A solution evolving into Q_* again explodes into multiple values upon exit from the

29

singularity, and while the flow inside $y_1 = y_2 = 0$ is more curved, it is the dynamics inside the layer on $y_2 = 0 \neq y_1$ that fundamentally alters the behaviour. Now, when re-collapse of the flow occurs on $y_2 = 0$, determinacy is only partialy restored, as the flow is torn in two, one part leaving the layer into $y_1, y_2 < 0$ as before, the other collapsing onto a sliding manifold on which block 2 sticks for a sustained interval. Ultimately block 2 also slips in this latter case too by reaching a turning point of the sliding manifold.

Thus in both cases, both blocks eventually slip, but now the micro-indeterminacy leads to a macroscopic indeterminacy — from the same initial condition passing through Q_* block 2 may or may not stick for a sustained interval of time, and begin slipping at a larger displacement $x_2 = -b_2$.

7 Closing remarks

The problem of coupled dry-friction oscillators has been studied before, of course, but attention has focussed on the complexity of their global dynamics, rather than on the sensitivity inside the discontinuity (sticking) surface that underlies it. We have shown here how a local singularity can be resolved that makes the transition from both blocks sticking, to both blocks slipping, indeterminate. Interestingly the indeterminacy re-collapses into a unique trajectory, but the microscopic break in determinacy both creates ambiguity in which block slips first, and manifests in local forces and global oscillations. If the oscillators are coupled via their discontinuous terms then we have shown that indeterminacy survives macroscopiccally, with trajectories splitting after the singularity into multiple streams.

The paper [28] begins an effort to classify deterministic and non-deterministic behaviour in nonsmooth dynamical systems by focusing on exit from sliding. Here we have presented a curious phenomenon of intermittent loss, bursts of indeterminacy on the micro-scale that are not *directly* observable in phase space variable on the macro-scale, but can nonetheless affect macro-scale quantities, namely the friction force felt during stick-slip events, and creating a bistability between global attractors.

References

[1] A. A. Andronov, A. A. Vitt, and S. E. Khaikin. *Theory of oscillations*. Moscow: Fizmatgiz (in Russian), 1959.

[2] J. Awrejcewicz, L. Dzyubak, and C. Grebogi. Estimation of chaotic and regular (stick-slip and slip-slip) oscillations exhibited by coupled oscillators with dry friction. *Nonlinear Dynamics*, 42:383–394, 2005.

[3] J. Awrejcewicz and D. Sendkowski. Stick-slip chaos detection in coupled oscillators with friction. *International Journal of Solids and Structures*, 42:5669–5682, 2005.

[4] A. Baule, H. Touchette, and E. G. D. Cohen. Stick–slip motion of solids with dry friction subject to random vibrations and an external field. *Nonlinearity*, 24:351–372, 2011.

[5] B. Bhushan. Contact mechanics of rough surfaces in tribology: multiple asperity contact. *Tribology Letters*, 4:1–35, 1998.

[6] P-A Bliman and M Sorine. Easy-to-use realistic dry friction models for automatic control. In *Proceedings of 3rd European Control Conference*, pages 3788–3794, 1995.

[7] Y. Braiman, F. Family, and H. G. E. Hentschel. Nonlinear friction in the periodic stick-slip motion of coupled oscillators. *Phys. Rev. B*, 55(8):491–5504, 1997.

[8] R. Burridge and L. Knopoff. Model and theoretical seismicity. *Bull. Seism. Soc. America*, 57(341– 371):629–656, 1967.

[9] C. Cantoni, R. Cesarini, G. Mastinu, G. Rocca, and R. Sicigliano. Brake comfort - a review. *Vehicle system dynamics: International Journal of Vehicle Mechanics and Mobility*, 27(8):901–947, 2009.

[10] J. M. Carlson and S. Langer. Mechanical model of an earthquake fault. *Phys. Rev. A*, 40:6470–6484, 1989.

[11] A. R. Champneys and P. L. Varkonyi. The Painleve paradox in contact mechanics. *IMA Journal of Applied Mathematics*, 81(3):538–88, 2016.

[12] I. Clancy and D. Corcoran. State-variable friction for the burridge-knopoff model. *Phys. Rev. E*, 80(016113):1–10, 2009.

[13] A. R. Crowther and R. Singh. Identification and quantification of stick-slip induced brake groan events using experimental and analytical investigations. *Noise Control Engineering Journal*, 56(4):235–255, 2008.

[14] G. Csernák and G. Stépán. On the periodic response of a harmonically excited dry friction oscillator. *Journal of Sound and Vibration*, 295:649–658, 2006.

[15] B. Derjaguin. Molekulartheorie der äusseren Reibung. *Zeitschrift für Physik*, 88(9-10):661–675, 1934.

[16] M. di Bernardo, P. Kowalczyk, and A. Nordmark. Sliding bifurcations: a novel mechanism for the sudden onset of chaos in dry friction oscillators. *Int.J.Bif.Chaos*, 13:2935–2948, 2003.

[17] B. Feeny and F.C. Moon. Chaos in a forced dry-friction oscillator: Experiments and numerical modelling. *J. Sound Vib.*, 170(3):303–323, 1994.

[18] N. Fenichel. Geometric singular perturbation theory. *J. Differ. Equ.*, 31:53–98, 1979.

[19] A. F. Filippov. *Differential Equations with Discontinuous Righthand Sides*. Kluwer Academic Publ. Dortrecht, 1988 (Russian 1985).

[20] U. Galvanetto. Bifurcations and chaos in a four-dimensional mechanical system with dry friction. *J. Sound Vib.*, 204:690–695(6), 1997.

[21] U. Galvanetto and S. R. Bishop. Dynamics of a simple damped oscillator undergoing stick-slip vibrations. *Meccanica*, 34:337–347, 1999.

[22] A. Guran, F. Pfeiffer, and K. Popp, editors. *Dynamics with Friction: Modeling, Analysis and Experiment I & II*, volume 7 of *Series B*. World Scientific, 1996.

[23] N. Hinrichs, M. Oestreich, and K. Popp. On the modelling of friction oscillators. *J. Sound Vib.*, 216(3):435–459, 1998.

[24] J. Huang and D. L. Turcotte. Evidence for chaotic fault interactions in the seismicity of the san andreas fault and nankai trough trough',. *Nature*, 348:234–236, 1990.

[25] J. Ing, E. Pavlovskaia, M. Wiercigroch, and S. Banerjee. Bifurcation analysis of an impact oscillator with a one-sided elastic constraints near grazing. *Physica D*, 239:312–321, 2010.

[26] M. R. Jeffrey. Hidden dynamics in models of discontinuity and switching. *Physica D*, 273-274:34–45, 2014.

[27] M. R. Jeffrey. On the mathematical basis of solid friction. *Nonlinear Dynamics*, 81(4):1699–1716, 2015.

[28] M. R. Jeffrey. Exit from sliding in piecewise-smooth flows: deterministic vs. determinacy-breaking. *Chaos*, 26(3):033108:1–20, 2016.

[29] M. R. Jeffrey. Hidden degeneracies in piecewise smooth dynamical systems. *Int. J. Bif. Chaos*, 26(5):1650087(1–18), 2016.

[30] M. R. Jeffrey. The ghosts of departed quantities in switches and transitions. *SIAM Review*, 60(1):116–36, 2017.

[31] M. R. Jeffrey and D. J. W. Simpson. Non-Filippov dynamics arising from the smoothing of nonsmooth systems, and its robustness to noise. *Nonlinear Dynamics*, 76(2):1395–1410, 2014.

[32] H. Jiang, A. S. E. Chong, Y. Ueda, and M. Wiercigroch. Grazing-induced bifurcations in impact oscillators with elastic and rigid constraints. *International Journal of Mechanical Sciences*, 127:204–14, 2017.

[33] C. K. R. T. Jones. *Geometric singular perturbation theory*, volume 1609 of *Lecture Notes in Math. pp. 44-120*. Springer-Verlag (New York), 1995.

[34] M. Kapitaniak, H. Vaziri, J. Paez Chavez, N. Krishnan, and M. Wiercigroch. Unveiling complexity of drill–string vibrations: Experiments and modelling. *International Journal of Mechanical Sciences*, 101-102:324–337, 2015.

[35] P. Kowalczyk and P.T. Piiroinen. Two-parameter sliding bifurcations of periodic solutions in a dry-friction oscillator. *Physica D: Nonlinear Phenomena*, 237(8):1053 – 1073, 2008.

[36] C. Kuehn. *Multiple time scale dynamics*. Springer, 2015.

[37] A. Le Bot and E. Bou Chakra. Measurement of friction noise versus contact area of rough surfaces weakly loaded. *Tribology Letters*, 37:273–281, 2010.

[38] E.M. Navarro-López and R. Suárez. Practical approach to modelling and controlling stick-slip oscillations in oilwell drillstrings. *Proceedings of the 2004 IEEE International Conference on Control Applications Taipei, Taiwan, September 2-4, 2004*, pages 1454–1460, 2004.

[39] D. N. Novaes and M. R. Jeffrey. Regularization of hidden dynamics in piecewise smooth flow. *J. Differ. Equ.*, 259:4615–4633, 2015.

[40] J. Nussbaum and A. Ruina. A two degree-of-freedom earthquake model with static/dynamic friction. *Pure and Applied Geophysics*, 125(4):629–656, 1987.

[41] M. Oestreich, N. Hinrichs, and K. Popp. Bifurcation and stability analysis for a non-smooth friction oscillator. *Archive of Applied Mechanics*, 301-314, 1996.

[42] H Olsson, K J Astrom, C C de Wit, M Gafvert, and P Lischinsky. Friction models and friction compensation. *Eur. J. Control*, 4:176–195, 1998.

[43] Persson, B. N. J. Albohr, U. O, Tartaglino, A. I. Volokitin, and E. Tosatti. On the nature of surface roughness with application to contact mechanics, sealing, rubber friction and adhesion. *J. Phys.: Condens. Matter*, 17:R1–R62, 2005.

[44] K. Popp and P. Stelter. Stick-slip vibrations and chaos. *Phil. Trans. R. Soc. A*, 332:89–105, 1990.

[45] T. Putelat, J. H. P. Dawes, and J. R. Willis. On the microphysical foundations of rate-and-state friction. *Journal of the Mechanics and Physics of Solids*, 59(5):1062–1075, 2011.

[46] C. Schoof. Marine ice-sheet dynamics. part 1. the case of rapid sliding. *J. Fluid Mech.*, 573:27–55, 2007.

[47] S. W. Shaw. On the dynamics response of a system with dry friction. *J. Sound Vib.*, 108(2):305–325, 1986.

[48] D. J. W. Simpson and R. Kuske. The positive occupation time of Brownian motion with two-valued drift and asymptotic dynamics of sliding motion with noise. *submitted*, 2013.

[49] D. J. W. Simpson and R. Kuske. Stochastically perturbed sliding motion in piecewise-smooth systems. *Discrete Contin. Dyn. Syst. Ser. B*, 19(9):2889–2913, 2014.

[50] J. Sotomayor and M. A. Teixeira. Regularization of discontinuous vector fields. *Proceedings of the International Conference on Differential Equations, Lisboa*, pages 207–223, 1996.

[51] M. A. Teixeira and P. R. da Silva. Regularization and singular perturbation techniques for non-smooth systems. *Physica D*, 241(22):1948–55, 2012.

[52] V. I. Utkin. *Sliding modes in control and optimization.* Springer-Verlag, 1992.

[53] M. Wechselberger. Existence and bifurcation of canards in $\mathbb{R}^3$ in the case of a folded node. *SIAM J. App. Dyn. Sys.*, 4(1):101–139, 2005.

[54] B. A. Wernitz and N. P. Hoffman. Recurrence analysis and phase space reconstruction of irregular vibration in friction brakes: Signatures of chaos in steady sliding. *J. Sound Vib.*, 331:3887–96, 2012.

[55] J. Wojewoda, S. Andrzej, M. Wiercigroch, and T. Kapitaniak. Hysteretic effects of dry friction: modelling and experimental studies. *Phil. Trans. R. Soc. A*, 366:747–765, 2008.

[56] J. Woodhouse, T. Putelat, and A. McKay. Are there reliable constitutive laws for dynamic friction? *Phil. Trans. R. Soc. A*, 373(20140401):1–21, 2015.